A versatile modular vector system for rapid combinatorial mammalian genetics

Albers, Joachim ; Danzer, Claudia ; Rechsteiner, Markus ; Lehmann, Holger ; Brandt, Laura P ; Hejhal, Tomas ; Catalano, Antonella ; Busenhart, Philipp ; Gonçalves, Ana Filipa ; Brandt, Simone ; Bode, Peter K ; Bode-Lesniewska, Beata ; Wild, Peter J ; Frew, Ian J

Abstract: Here, we describe the multiple lentiviral expression (MuLE) system that allows multiple genetic alterations to be introduced simultaneously into mammalian cells. We created a toolbox of MuLE vectors that constitute a flexible, modular system for the rapid engineering of complex polycistronic lentiviruses, allowing combinatorial gene overexpression, gene knockdown, Cre-mediated gene deletion, or CRISPR/Cas9-mediated (where CRISPR indicates clustered regularly interspaced short palindromic repeats) gene mutation, together with expression of fluorescent or enzymatic reporters for cellular assays and animal imaging. Examples of tumor engineering were used to illustrate the speed and versatility of performing combinatorial genetics using the MuLE system. By transducing cultured primary mouse cells with single MuLE lentiviruses, we engineered tumors containing up to 5 different genetic alterations, identified genetic dependencies of molecularly defined tumors, conducted genetic interaction screens, and induced the simultaneous CRISPR/Cas9-mediated knockout of 3 tumor-suppressor genes. Intramuscular injection of MuLE viruses expressing oncogenic H-RasG12V together with combinations of knockdowns of the tumor suppressors cyclin-dependent kinase inhibitor 2A (Cdkn2a), transformation-related protein 53 (Trp53), and phosphatase and tensin homolog (Pten) allowed the generation of 3 murine sarcoma models, demonstrating that genetically defined autochthonous tumors can be rapidly generated and quantitatively monitored via direct injection of polycistronic MuLE lentiviruses into mouse tissues. Together, our results demonstrate that the MuLE system provides genetic power for the systematic investigation of the molecular mechanisms that underlie human diseases.

DOI: https://doi.org/10.1172/JCI79743

A versatile modular vector system for rapid combinatorial mammalian genetics

Joachim Albers,[1] Claudia Danzer,[1] Markus Rechsteiner,[2] Holger Lehmann,[1] Laura P. Brandt,[1] Tomas Hejhal,[1] Antonella Catalano,[1] Philipp Busenhart,[1] Ana Filipa Gonçalves,[1] Simone Brandt,[2] Peter K. Bode,[2] Beata Bode-Lesniewska,[2] Peter J. Wild,[2] and Ian J. Frew[1,3]

[1]Institute of Physiology, University of Zurich, Zurich, Switzerland. [2]Institute of Surgical Pathology, University Hospital Zurich, Zurich, Switzerland. [3]Zurich Center for Integrative Human Physiology, University of Zurich, Zurich, Switzerland.

Here, we describe the multiple lentiviral expression (MuLE) system that allows multiple genetic alterations to be introduced simultaneously into mammalian cells. We created a toolbox of MuLE vectors that constitute a flexible, modular system for the rapid engineering of complex polycistronic lentiviruses, allowing combinatorial gene overexpression, gene knockdown, Cre-mediated gene deletion, or CRISPR/Cas9-mediated (where CRISPR indicates clustered regularly interspaced short palindromic repeats) gene mutation, together with expression of fluorescent or enzymatic reporters for cellular assays and animal imaging. Examples of tumor engineering were used to illustrate the speed and versatility of performing combinatorial genetics using the MuLE system. By transducing cultured primary mouse cells with single MuLE lentiviruses, we engineered tumors containing up to 5 different genetic alterations, identified genetic dependencies of molecularly defined tumors, conducted genetic interaction screens, and induced the simultaneous CRISPR/Cas9-mediated knockout of 3 tumor-suppressor genes. Intramuscular injection of MuLE viruses expressing oncogenic *H-Ras*^{G12V} together with combinations of knockdowns of the tumor suppressors cyclin-dependent kinase inhibitor 2A (*Cdkn2a*), transformation-related protein 53 (*Trp53*), and phosphatase and tensin homolog (*Pten*) allowed the generation of 3 murine sarcoma models, demonstrating that genetically defined autochthonous tumors can be rapidly generated and quantitatively monitored via direct injection of polycistronic MuLE lentiviruses into mouse tissues. Together, our results demonstrate that the MuLE system provides genetic power for the systematic investigation of the molecular mechanisms that underlie human diseases.

Introduction

In the study of many biological processes, it is often desirable to be able to genetically manipulate multiple genes simultaneously. A prime example is tumor modeling in mice. The application of genomic technologies to the study of cancers has revolutionized our understanding of the genetic landscapes of tumors (1, 2); however, functional studies are required to make sense of these cataloguing efforts to determine how different combinations of the many candidate genetic mutations dictate tumor phenotypes and to provide accurate models that can be used in preclinical studies to identify mutation-specific therapies. Germline genetic manipulation techniques have allowed the generation of lines of mice in which genes can be deleted, mutated, silenced, or overexpressed in temporal and cell-type–specific manners (3). These approaches have provided many insights into cancer development and progression; however, the generation of genetically modified mice and their interbreeding to generate compound mutants are time consuming and costly processes. In addition, tumor modeling ex vivo using primary cells is often complicated by the limited period for which these cells can be cultured and the lack of appropriate genetic tools that allow multiple genetic alterations to be introduced simultaneously into these cells. Current gene-delivery approaches aiming to introduce multiple genetic alterations using plasmid or viral vectors often require cumbersome cloning approaches to generate complicated multicistronic vector constructs and/or multiple rounds of transfection or transduction and necessitate the introduction of multiple selective markers to identify and isolate the appropriate cells.

To address these issues, we have developed the multiple lentiviral expression (MuLE) system, which is based on MultiSite Gateway cloning (4) and allows the easy and flexible generation of polycistronic, replication-incompetent ecotropic or amphotropic lentiviruses. This system allows complex combinatorial genetic alterations to be introduced into mammalian cells by infection ex vivo and in vivo with a single vector. The use of lentiviral gene delivery permits the transduction of a wide variety of dividing and nondividing cells, and the integration of the provirus into the genome provides heritability of the introduced genetic alterations. We present examples of cancer engineering ex vivo and in vivo to demonstrate that this system, when used alone or in combination with germline genetic approaches, provides new experimental genetic power in cultured mammalian cells and in mice.

Results

Generation of complex polycistronic lentiviruses using the MuLE vector toolbox. To be able to quickly and systematically conduct combinatorial genetic experiments in cultured mammalian cells and

Conflict of interest: The authors have declared that no conflict of interest exists.
Submitted: December 19, 2014; **Accepted:** January 20, 2015.
Reference information: *J Clin Invest*. 2015;125(4):1603–1619. doi:10.1172/JCI79743.

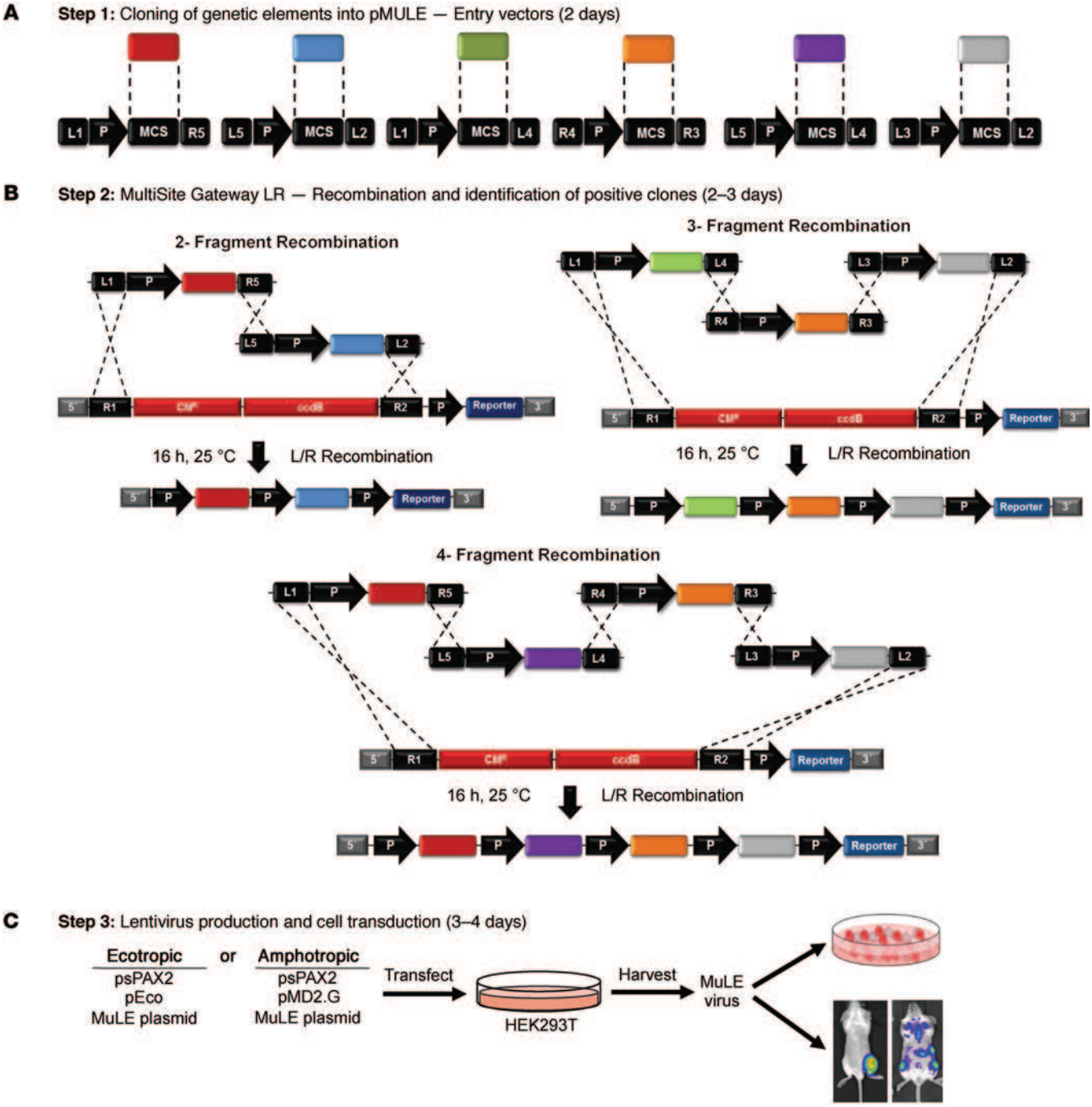

Figure 1. Overview of genetic engineering experiments using MuLE vectors. (**A**) Restriction enzyme cloning is used to generate MuLE Entry vectors with a desired genetic insert cloned downstream of a desired promoter (P), with the entire promoter-insert element being surrounded by appropriate attL-attR sites. (**B**) Schematic overview of the MultiSite Gateway–based recombination cloning of 2, 3, or 4 MuLE Entry vectors into lentiviral destination vectors to generate multicistronic MuLE lentiviral expression vectors. The specific attL-attR sites that mediate each recombination are depicted. CM^R, chloramphenicol resistance gene; ccdB, ccdB toxin gene. (**C**) Transfection of 293T cells with a MuLE expression vector plasmid together with a lentiviral packaging vector (psPAX2) and a vector encoding either amphotropic (MD2G) or ecotropic (pEco) envelope proteins generates MuLE lentiviruses for transduction of cultured cells or for in vivo injection into mouse tissues.

in mouse tissues, we designed a genetic system that allows complex lentiviral gene-delivery vectors to be generated in a very flexible, rapid, and user-friendly manner. We generated a toolbox of building-block vectors that allows multiple genetic elements to be combinatorially recombined into a family of lentiviral gene-delivery vectors. A series of 104 MultiSite Gateway–compatible Entry vectors (MuLE Entry vectors, Supplemental Tables 1 and 2; supplemental material available online with this article; doi:10.1172/JCI79743DS1) that allow several different types of genetic manipulations has been generated. Conventional restriction enzyme clon-

ing is first used to clone genetic inserts downstream of a promoter of choice, with the entire promoter-insert genetic element being flanked by specific attL and attR sites (Figure 1A). MuLE Entry vectors can be recombined efficiently in an overnight reaction via an attL-attR recombination with a variety of Gateway destination lentiviral vectors that we have generated. The choice of different attL-attR sites provides directional specificity to the recombination reactions and allows either 1, 2, 3, or 4 MuLE Entry vectors to be simultaneously recombined into the Destination vector. Using this system, complex multicistronic mammalian expression vectors containing 2, 3, 4, or 5 independent genetic elements can be rapidly generated (Figure 1B). MuLE vectors can be packaged to generate amphotropic or ecotropic lentiviruses, which can then be used for infection of cultured cell lines, primary cells ex vivo or cells in mouse tissues in vivo (Figure 1C). This entire procedure can be completed within 7 to 8 days.

We generated Entry vectors containing 3 different RNA polymerase (pol) II promoters (CMV, SV40, SFFV) and a multiple cloning site (MCS) to generate genetic elements allowing constitutive cDNA overexpression (Figure 2A). An Entry vector with a CMV promoter and *lox*P sites flanking the MCS allows for Cre-mediated conditional removal of inserted genes (Figure 2A) and Entry vectors containing a doxycycline-inducible (DOX-inducible) CMV/TO promoter allow inducible gene expression (Figure 2B). Supplemental Table 3 shows the restriction enzyme sites of the MCS of each vector. Promoterless Entry vectors containing only a MCS flanked by different combinations of attL-attR sites (Figure 2C) represent flexible elements that facilitate the generation of diverse types of complex vector constructs. We generated Entry vectors to allow U6 promoter–driven expression of short guide RNAs (sgRNAs) for CRISPR/Cas9-mediated (where CRISPR indicates clustered regularly interspaced short palindromic repeats) gene mutation (Figure 2D). Entry vectors with 3 different constitutive pol III promoters (U6, 7SK, H1) allowed the expression of shRNAs (Figure 2E). For constitutive expression of shRNAs in microRNA-30 (miR-30) format, we generated Entry vectors based on the pSM2 plasmid (5), which includes the 5′ and 3′ flanking sequences from miR-30 driven by the U6, 7SK, or H1 pol III promoters (Figure 2F). A DOX-inducible gene knockdown vector was generated by using the CMV/TO promoter to drive shRNA–miR-30 expression (Figure 2G). In addition to these flexible cloning vectors, we created several ready-to-use Entry vectors containing cDNAs for hCas9, fluorescent proteins (EGFP, mCherry, near-infrared fluorescent protein [iRFP], tdTomato), enzymatic reporters (luciferase, lacZ), drug resistance (puromycin), and tamoxifen-inducible Cre recombinase (Cre-ER^{T2}) (Figure 2H). To allow a high degree of flexibility in combining different numbers and types of Entry vectors by recombination cloning, most of the described vectors are available with multiple combinations of different attL-attR sites (Supplemental Tables 1 and 2). We further extended our vector toolbox by generating a series of lentiviral Destination vectors based on modifications of the previously described pLenti X1-Puro-DEST vector (6), allowing cells to be marked with drug resistance (puromycin, neomycin) or a variety of fluorescent (EGFP, iRFP, IFP1.4) or luminescent (luciferase) proteins (Figure 2I) to facilitate cellular assays as well as live animal-imaging studies. We performed numerous recombination reactions with the MuLE system and found that approximately 90%, 65%, or 25% of all bacterial colonies isolated from recombinations involving 2, 3, or 4 Entry vectors, respectively, contained the desired product (Figure 2J). Thus, highly complicated, multicistronic MuLE expression vectors can be easily cloned. These complex vectors can be stably replicated in bacteria and show no evidence of unwanted genetic recombination (Supplemental Figure 1). Similarly to all lentiviral vectors, there is an inverse relationship between the size of the MuLE provirus and the titer of the generated virus, with proviruses up to 7.5 kb yielding titers of approximately 10^6 CFU/ml and very large (12.5 kb) proviruses yielding titers of approximately 10^3 CFU/ml (Supplemental Figure 2). All of these vectors have been deposited with Addgene and can be obtained individually or as a 96-vector set. Addgene reference numbers for each vector are provided in Supplemental Tables 1 and 2.

While the MuLE system is compatible with the VSV-G amphotropic envelope protein (Supplemental Figure 5 shows an example), for biosafety reasons, all lentiviruses used to transduce murine cells in this study were pseudotyped with an ecotropic envelope protein from the Moloney murine leukemia virus that has been described as allowing lentiviral infection of murine fibroblast and hematopoietic cells, but not of human cells (7, 8). Despite obvious biosafety advantages, this envelope has surprisingly found very little use in research laboratories. We further examined the cellular tropism of MuLE lentiviruses pseudotyped with this envelope and found that they infect a variety of cultured primary cells, including mouse embryonic fibroblasts (MEFs), embryonic stem cells, kidney epithelial cells, endometrial epithelial cells, hepatocytes, and aortic endothelial cells as well as immortalized myoblast, melanoma, lung carcinoma, and colorectal carcinoma cell lines, but were not able to infect several human cell lines, including 786-O, 293T (Figure 3A), HeLa, and MCF-7 (data not shown). Cell-type–specific gene expression is also possible using MuLE vectors. Cloning EGFP downstream of the renal epithelium–specific Ksp1.3 promoter in a MuLE vector (Figure 3B) allowed expression of EGFP in renal epithelial cells but not in MEFs (Figure 3C). Thus, ecotropic MuLE viruses can infect a broad spectrum of target cells and can be utilized to induce gene expression in a cell-type–specific manner.

In order to validate the functionality of the vector toolbox for the genetic manipulation of primary cells, we conducted a series of experiments involving transduction of primary MEFs. Unless otherwise stated, all experiments in this publication were conducted at an MOI of 1. These validation studies demonstrated that MuLE vectors are capable of the following: (a) inducing shRNA-mediated knockdown from different pol III promoters (Supplemental Figure 3, A–C); (b) inducing simultaneous double-gene knockdowns from a single vector in a manner in which the strengths of the knockdowns are independent of the order of the knockdown cassettes in the vector (Supplemental Figure 3, D and E) and are equivalent to the extent of knockdowns obtained from vectors expressing the single shRNAs (Supplemental Figure 3, F and G); (c) inducing shRNA–miR-30–mediated constitutive (Supplemental Figure 3, H–J) and inducible (Supplemental Figure 3, K–M) gene knockdown; (d) inducing tamoxifen-inducible Cre-ER^{T2}–mediated gene deletion (Supplemental Figure 4, A and B); and (e) inducing the

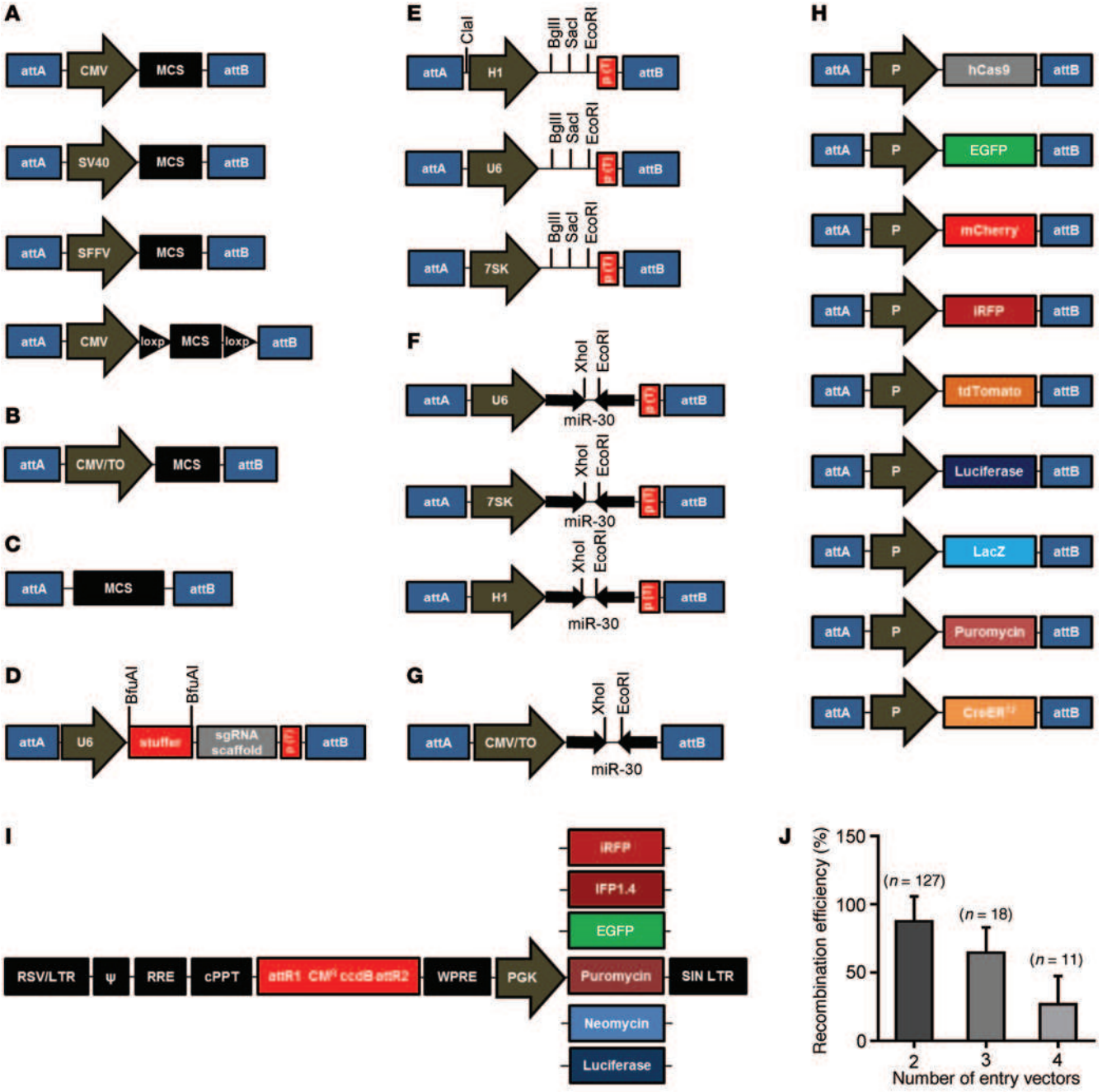

Figure 2. The MuLE vector toolbox. (**A** and **B**) MuLE Entry vectors for pol II promoter–driven constitutive expression (**A**) or DOX-inducible expression (**B**). (**C**) Promoterless MuLE Entry vectors. (**D**) MuLE Entry vectors for U6-driven expression of sgRNAs. (**E** and **F**) MuLE Entry vectors for shRNA-based (**E**) and shRNA–miR-30–based (**F**) gene knockdown using pol III promoters and (**G**) a DOX-inducible miR-30–based shRNA expression vector. Restriction enzyme sites for cloning are shown. (**H**) Schematic representation of MuLE Entry vectors for expression of hCas9, fluorescent proteins (EGFP, mCherry, iRFP, tdTomato), firefly-luciferase, β-galactosidase (LacZ), puromycin resistance, or Cre-ER^{T2}. P, various promoters. In all panels, attA and attB denote that multiple combinations of MultiSite Gateway attL-attR sites are available for these vectors. (**I**) Schematic representation of Destination vectors modified from the pLenti X1 series to contain the different expression cassettes shown. (**J**) Quantification (mean ± SD) of recombination efficiencies of *n* independent MultiSite Gateway attL-attR recombinations using 2, 3, or 4 MuLE Entry vectors.

simultaneous expression of 2 shRNAs, 2 cDNAs, and a drug-resistance gene from 5 different expression cassettes in a single vector (Supplemental Figure 4, C–E). Transduction of human A-375 melanoma cells showed that MuLE viruses expressing iRFP or luciferase proteins allow quantitative monitoring of tumor burden in xenograft experiments (Supplemental Figure 5).

Engineering genetically complex tumors from primary cells using single MuLE viruses. To demonstrate the utility of the MuLE system in cancer modeling, we performed experiments in MEFs showing that a single virus can reproduce several phenotypes that are known to result from genetic cooperation between oncogenes and tumor-suppressor genes. Overexpression of an oncogenic form of

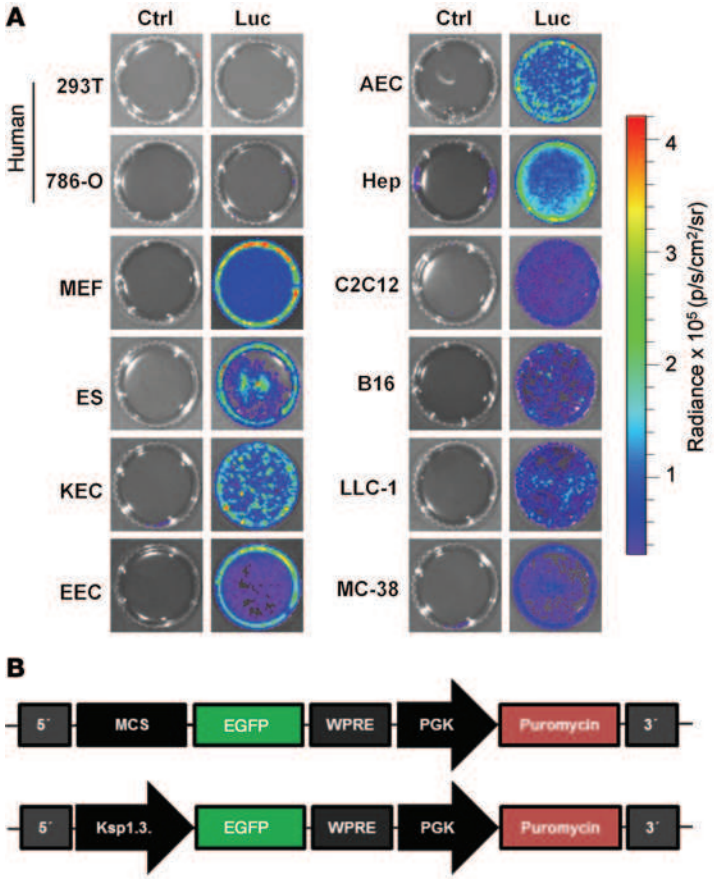

Figure 3. Broad cellular tropism and cell-type–specific expression of ecotropic MuLE vectors. (**A**) Luminescent imaging of various human and mouse cultured cells after infection with ecotropic MuLE viruses expressing an empty cassette (Ctrl) or luciferase (Luc). The human kidney cell lines 293T and 786-0 were not infected by these viruses, but various primary mouse cells and cell lines were infected, including MEFs, embryonic stem cells (ES), kidney epithelial cells (KEC), endometrial epithelial cells (EEC), aortic endothelial cells (AEC), hepatocytes (Hep), myoblasts (C2C12), melanoma cells (B16), lung carcinoma cells (LLC-1), and colorectal carcinoma cells (MC-38). (**B**) Schematic of MuLE vectors with or without the kidney epithelium–specific Ksp1.3 promoter cloned upstream of a cDNA encoding EGFP. (**C**) Representative bright field (BF) and green fluorescence (EGFP) images of primary mouse kidney epithelial cells (PKCs) and primary MEFs transduced with the lentiviral vectors shown in **B**. Original magnification, ×1 (**A**); ×10 (**C**).

H-Ras (G12V) in combination with loss of function of p53 results in cellular transformation (9, 10). We generated a tricistronic lentiviral expression vector designed to simultaneously express shRNA–miR-30 against transformation-related protein 53 (*Trp53*) and express oncogenic *H-Ras*^{G12V} and puromycin resistance (Figure 4A) as well as control viruses expressing neither or only 1 of these elements. Western blot analysis of puromycin-selected primary MEFs demonstrated the expected knockdown of p53 and overexpression of H-Ras^{G12V} (Figure 4B), and transformation assays demonstrated that *Trp53* knockdown alone allowed colony formation following plating at low density (Figure 4C), but that loss of contact inhibition (foci formation) and anchorage-independent growth occurred only in cells with simultaneous knockdown of *Trp53* and overexpression of *H-Ras*^{G12V}, as expected (Figure 4, D–F). Similarly, the use of a single MuLE vector to simultaneously knock down *Trp53* and overexpress *Myc* (Figure 4, G and H) allowed growth of cells at low density (Figure 4I) and reproduced the known effect of loss of *Trp53* function in rescuing *Myc*-induced apoptosis in MEFs (ref. 11 and Figure 4J).

To further prove the utility of our system in tumor modeling, we generated a multicistronic vector designed to knock down *Trp53*, overexpress *H-Ras*^{G12V} from the inducible CMV/TO promoter, and express iRFP to allow monitoring of tumor development (Figure 5A). Blasticidin-resistant MEFs after infection with pLenti-CMV-TetR-Blast (6) were transduced with the MuLE vector and selected with puromycin. Western blot analysis indicated constitutive p53 knockdown, but H-Ras^{G12V} overexpression occurred only upon induction with DOX (Figure 5B). These cells grew efficiently as tumors when injected subcutaneously in immunocompromised SCID/beige mice only upon addition of DOX to the drinking water (Figure 5, C–E), demonstrating that MuLE vectors can be employed to generate regulatable and quantitatively monitorable models of cancer based on cooperative genetic interactions.

To further demonstrate the potential of MuLE vectors for engineering and monitoring genetically complex tumors, we generated a pentacistronic vector to simultaneously express shRNA–miR-30 against the Retinoblastoma (*Rb1*) tumor-suppressor gene and shRNA against the phosphatase and tensin homolog (*Pten*) tumor-suppressor gene as well as to express oncogenic *H-Ras*^{G12V}, Cre-ER^{T2}, and the puromycin resistance gene (Figure 6A). We transduced (MOI = 2) primary MEFs harboring floxed alleles of the von Hippel–Lindau (*Vhl*) and *Trp53* genes (*Vhl*$^{fl/fl}$ *Trp53*$^{fl/fl}$) and treated puromycin-selected cells with 300 nM 4-hydroxytamoxifen (4-OHT) or vehicle for a period of 3 days. Cells transduced with the lentivirus and treated with 4-OHT showed reduction of VHL abundance (accompanied by stabilization of HIF1A), reduction of PTEN, pRb, and p53 protein levels, and overexpression of H-Ras^{G12V}, (Figure 6B) thus demonstrating the functionality of each expression cassette in the MuLE vector. To analyze the potential of these cells to form genetically defined tumors in vivo, we additionally transduced the cells with a MuLE virus expressing EGFP and iRFP, thereby generating within 1 week pools of cells that harbored 5 separate genetic changes and expression of 3 marker genes. Cells that were treated with 4-OHT grew marginally faster in xenograft

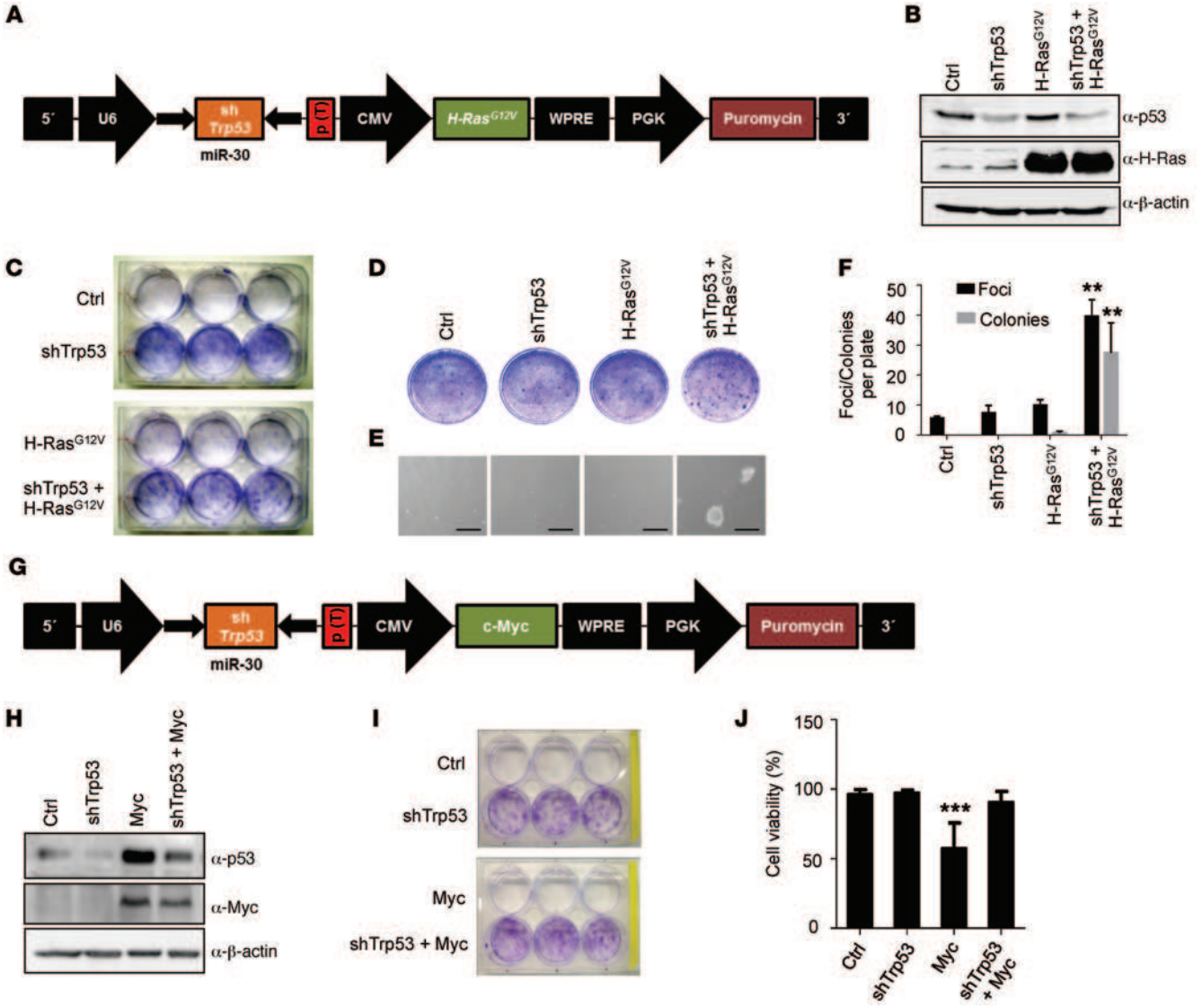

Figure 4. Combinatorial genetics using MuLE vectors. (**A**) Lentiviral vector to simultaneously knock down *Trp53* and overexpress oncogenic *H-Ras*^{G12V}. (**B**) Western blot analysis of primary MEFs transduced with the indicated lentiviruses. (**C**) Crystal violet staining of the same cells 14 days after seeding at low density and (**D**) 14 days after seeding in a focus formation assay. (**E**) Representative images of the same cells seeded in a soft agar colony assay after 3 weeks of growth. Scale bars: 200 μm. (**F**) Quantification of the foci and colonies growing in assays from **D** and **E**. (**G**) Lentiviral vector generated to simultaneously knock down *Trp53* and overexpress Myc. (**H**) Western blot analysis of primary MEFs transduced with the indicated lentiviruses. (**I**) Crystal violet staining of the same cells 14 days after seeding at low density. (**J**) Quantification of viable cells 3 days after transduction with the indicated lentiviruses. All graphs depict mean ± SD. Student's *t* test, $n = 3$. $^{**}P < 0.01$; $^{***}P < 0.001$.

assays than those that were not treated (Figure 6C and Supplemental Figure 6, A and B). Importantly, cells that were isolated from the tumors 3 weeks after injection retained EGFP expression (data not shown) and displayed the same changes in protein abundance that were present in the cells before injection (Figure 6D), demonstrating that MuLE viruses permit the introduction of stable genetic alterations.

We took advantage of this system to perform proof-of-principle therapeutic target identification experiments to show that MuLE viruses can be employed to assess which genes are necessary for the growth of tumors with a defined set of genetic mutations. Using the same work flow described above, we infected primary MEFs derived from WT, *Hif1a*$^{fl/fl}$, *Hif2a*$^{fl/fl}$, or *Hif1a*$^{fl/fl}$ *Hif2a*$^{fl/fl}$ mice with the virus shown in Figure 6A to assess the contribution of the hypoxia-inducible factor α (HIF1α and HIF2α) transcription factors to tumor development in the background of oncogenic *H-Ras*^{G12V} together with loss of function of *Rb1* and *Pten*. mRNA analyses confirmed that 4-OHT treatment induced the anticipated downregulation of *Hif1a* and/or *Hif2a* and of several *Hif1a* target genes in these cells (Figure 7A). Xenograft experiments revealed that HIF1α, but not HIF2α, is necessary for efficient tumor growth in this model (Figure 7, B–E). All tumors described in Figures 6 and 7 displayed a similar histological appearance of sarcomatoid cells growing in a storiform pattern, with numerous tumor giant cells with bizarre nuclei (Supplemental Figure 6, C and D). We took advantage of this large set of imaging data to perform an analysis of the utility of iRFP to monitor tumor growth. iRFP is a new fluorescent protein that has been proposed to be

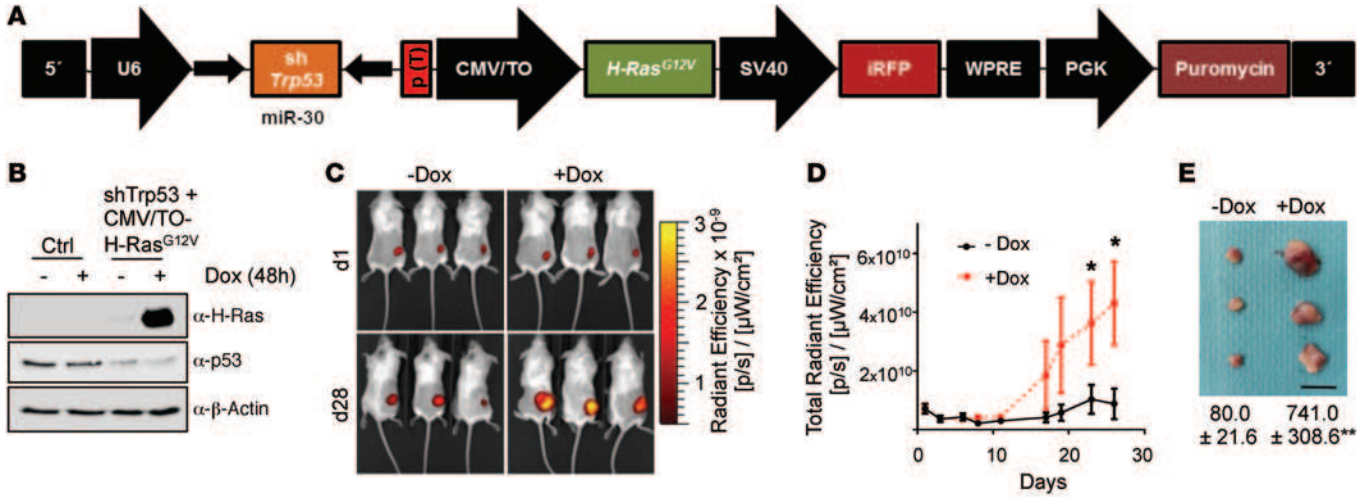

Figure 5. Combinatorial genetics using inducible MuLE vectors. (**A**) Multicistronic lentiviral vector to simultaneously knock down *Trp53*, overexpress inducible *H-Ras*^{G12V}, and overexpress iRFP. (**B**) Western blot analysis demonstrating H-Ras^{G12V} overexpression in TetR-expressing MEFs transduced with the lentivirus shown in **A** upon addition of 1 μM DOX to the culture medium. (**C**) In vivo fluorescence imaging of mice that were subcutaneously injected with shRNA-Trp53/CMV/TO-H-Ras^{G12V} MuLE virus–infected MEFs and fed drinking water without or with DOX. (**D**) Longitudinal tumor growth quantified by iRFP fluorescence imaging. (**E**) Image of the isolated tumors and tumor weight after 28 days. Scale bar: 1 cm. Student's *t* test, $n = 3$. $^*P < 0.05$; $^{**}P < 0.01$.

excellent for animal imaging due to the low absorbance by mouse tissues of the emitted light (12–14). In each of the 5 experiments described above, there was a strong linear correlation between the iRFP signal and the measured tumor volume over time, with Pearson correlation coefficient R^2 values ranging from 0.79 to 0.94 in the experiments (Supplemental Figure 6E), supporting the utility of iRFP as an excellent marker protein to track tumor formation and progression in mouse imaging studies.

Combinatorial CRISPR/Cas9-mediated genetic engineering using single MuLE vectors. The discovery of the applicability of the CRISPR/Cas9 system to mammalian cells has provided a powerful new tool to efficiently target genetic mutations to defined loci (15, 16), and very recent publications illustrate the power of this system for tumor engineering in mice (17–20). We reasoned that the ease and flexibility of cloning provided by the MuLE system would make it an ideal experimental platform to generate vectors that allow the introduction of multiple simultaneous genetic manipulations using CRISPR/Cas9. We first generated tricistronic MuLE vectors expressing single sgRNAs targeting exon 7 or exon 8 of the *Trp53* locus or exon 2 of the cyclin-dependent kinase inhibitor 2A (*Cdkn2a*) locus together with expression of *hCas9* and puromycin resistance (Supplemental Figure 7A) and infected primary MEFs. Two functionally validated *Trp53* sgRNAs (21) and 3 newly designed *Cdkn2a* sgRNAs, but not a scrambled control sgRNA (21), induced efficient mutation of their respective target genes, as shown by Surveyor assays (Supplemental Figure 7B). Both *Trp53* sgRNAs caused the generation of truncated p53 protein species, and 2 of 3 *Cdkn2a* sgRNAs caused loss of p16 and p19 protein expression (Supplemental Figure 7C), verifying that CRISPR/Cas9 genome engineering is compatible with the MuLE system.

To demonstrate that cooperative genetic tumor modeling can be achieved using CRISPR/Cas9-mediated gene knockout together with oncogene overexpression from a single vector, we generated tetracistronic MuLE vectors designed to express either scrambled sgRNA or sgRNAs targeting *Trp53* exon 7 or exon 8 as well as to express *H-Ras*^{G12V}, *hCas9*, and puromycin resistance (Figure 8A) and used these to infect primary MEFs. All viruses expressing sgRNA against *Trp53*, but not the control virus, allowed colony formation following plating of cells at low density (Figure 8B), but tumor formation in xenograft assays only resulted from the combination of sgRNA against *Trp53* with *H-Ras*^{G12V} expression (Figure 8C). Western blotting of independent cell lines isolated from independent tumor xenografts of each genotype confirmed the overexpression of H-Ras^{G12V} and the presence of numerous truncated mutant p53 protein species (Figure 8D).

Previous approaches using the CRISPR/Cas9 system to generate cells harboring multiple mutations required the cotransfection of multiple plasmids, the simultaneous infection with multiple viruses, and the use of transgenic mice that express hCas9 or that carry germline floxed alleles (17, 18, 20, 22, 23). The multicistronic building-block MuLE viral system allows multiple sgRNAs to be expressed together with *hCas9* from a single viral construct. To prove that this approach of targeting multiple loci simultaneously with a single vector is feasible, we generated pentacistronic MuLE viruses, each simultaneously expressing sgRNAs against the *Trp53*, *Pten*, and *Vhl* tumor-suppressor genes, *hCas9*, and puromycin resistance (Figure 8E). Two different sgRNAs targeting *Trp53* exon 7 or exon 8, 3 different sgRNAs targeting *Pten* exon 1 or exon 2, and 3 different sgRNAs targeting *Vhl* exon 1 were combined to generate 3 independent MuLE viruses expressing different sets of sgRNAs. After infection and selection for drug resistance, cells were plated at low density to assess cellular transformation. All viruses allowed the formation of colonies (Figure 8F), indicative of loss of p53 function, and a total of 21 clonal immortalized cell lines were derived from isolated colonies. Western blotting revealed the complete loss or reduction of expression of PTEN and VHL and presence of truncated p53 protein species in 16, 14, and 20 clones, respectively (Figure 8G). All clones displayed levels

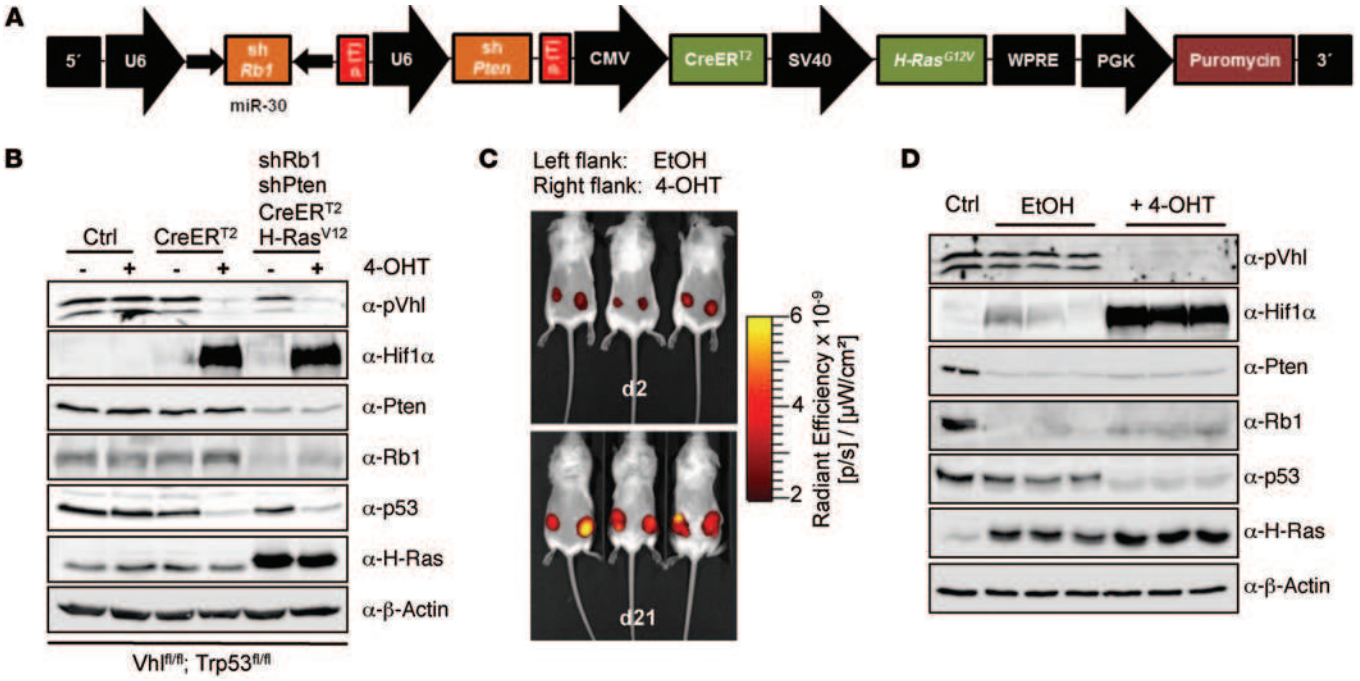

Figure 6. Generation of genetically complex tumors with multicistronic MuLE vectors. (**A**) Pentacistronic vector to simultaneously knock down *Rb1* and *Pten* and to express CreER^{T2}, oncogenic *H-Ras^{G12V}*, and puromycin resistance. (**B**) Western blot analysis of puromycin-selected *Vhl$^{fl/fl}$ Trp53$^{fl/fl}$* primary MEFs that were transduced with lentivirus shown in **A**, virus containing 4 empty inserts (Ctrl), or 3 empty inserts plus CreER^{T2}, and treated with 300 nM 4-OHT or ethanol (EtOH) for 4 days. (**C**) In vivo fluorescence images of mice taken 2 and 21 days after subcutaneous injection of *Vhl$^{fl/fl}$ Trp53$^{fl/fl}$* MEFs transduced with lentivirus generated from the vector shown in **A** that had been treated with EtOH (left flank) or with 4-OHT (right flank) prior to injection. (**D**) Western blot analysis of tumor cells that were isolated from 3 separate tumors of each genotype 3 weeks after cell injection.

of the p53-inducible p21 protein equivalent to levels in *Vhl/Trp53* null MEFs, verifying that functional p53 knockout occurred in all clones. Sixteen clones displayed stabilization of HIF1α protein, and 14 clones displayed elevated levels of P-S473-Akt, indicative of functional loss of VHL and PTEN, respectively (Figure 8G). Since some clones retained protein expression of p53, VHL, and/or PTEN, we further validated that mutations arose at all loci by using deep sequencing to genotype the regions of *Pten*, *Trp53*, and *Vhl* targeted by the sgRNAs in each of 10 clones (Table 1). Half of the clones showed insertions or deletions of all 6 alleles, and half showed mutations of 5 of 6 alleles, demonstrating that infection with a single MuLE CRISPR/Cas9 vector can simultaneously induce mutations in multiple target genes.

Combinatorial genetic screening using MuLE vectors. Another advantage of the building-block nature of the MuLE system is that it provides a platform to facilitate population-based genetic interaction screens. As proof of principle that this is feasible, we conducted a screen to identify negative regulators of the cell cycle whose loss of function can cooperate with H-Ras^{G12V} to allow transformation of MEFs. We assembled an shRNA library (designated shRNA X) in the commercially available pLKO.1 vector backbone, comprising 4 to 6 shRNAs against each member of the *Cdkn1*, *Cdkn2*, *Trp53*, and *Rb* gene families (Figure 9A). PCR was used to amplify all shRNAs, including the U6 promoter, from a pooled DNA preparation of this library, and the product was cloned en masse into a MuLE Entry vector to generate an Entry shRNA X library, which was recombined to generate a library of tricistronic MuLE vectors, each expressing a single shRNA from the library together with *H-Ras^{G12V}* and EGFP. These MuLE vectors and control vectors expressing either nonsilencing shRNA, the shRNA X library alone, or *H-Ras^{G12V}* alone were transduced into MEFs at an MOI of 0.1 to avoid multiple integrations into the same cell. Transduced cells were plated at low density in the presence of a 30-fold excess of WT MEFs for a focus formation assay. The combination of the shRNA X library plus *H-Ras^{G12V}* resulted in an increased number of foci (Figure 9B). Eight EGFP-positive foci were isolated and expanded as cell lines. PCR followed by DNA sequencing was used to isolate and identify the integrated shRNA, revealing that 7 of these clones contained shRNA against *Cdkn2a* (clone TRCN0000222731) and 1 contained shRNA against *Trp53* (clone TRCN0000012360). Western blotting verified the knockdown of p19 and p16 protein expression in the *Cdkn2a* shRNA–expressing cell lines and of p53 in the *Trp53* shRNA–expressing cell line (Figure 9C). Reengineering MuLE viruses to express the isolated *Cdkn2a* shRNA together with *H-Ras^{G12V}* and iRFP expression cassettes, as well as relevant control viruses, confirmed that this genetic cooperation causes transformation of MEFs and allows these cells to grow as xenografts in immunocompromised mice (Figure 9, D and E). Loss of function of *Cdkn2a* or of *Trp53* has been shown to cooperate with activated H-Ras in causing transformation of MEFs (24), validating the effectiveness of screening for cooperative genetic events with the MuLE system.

Generation of genetically complex, quantitatively monitorable autochthonous sarcomas in mice using single MuLE viruses. Having established the power of the MuLE system for combinatorial genetics in primary cells ex vivo and based on experiments show-

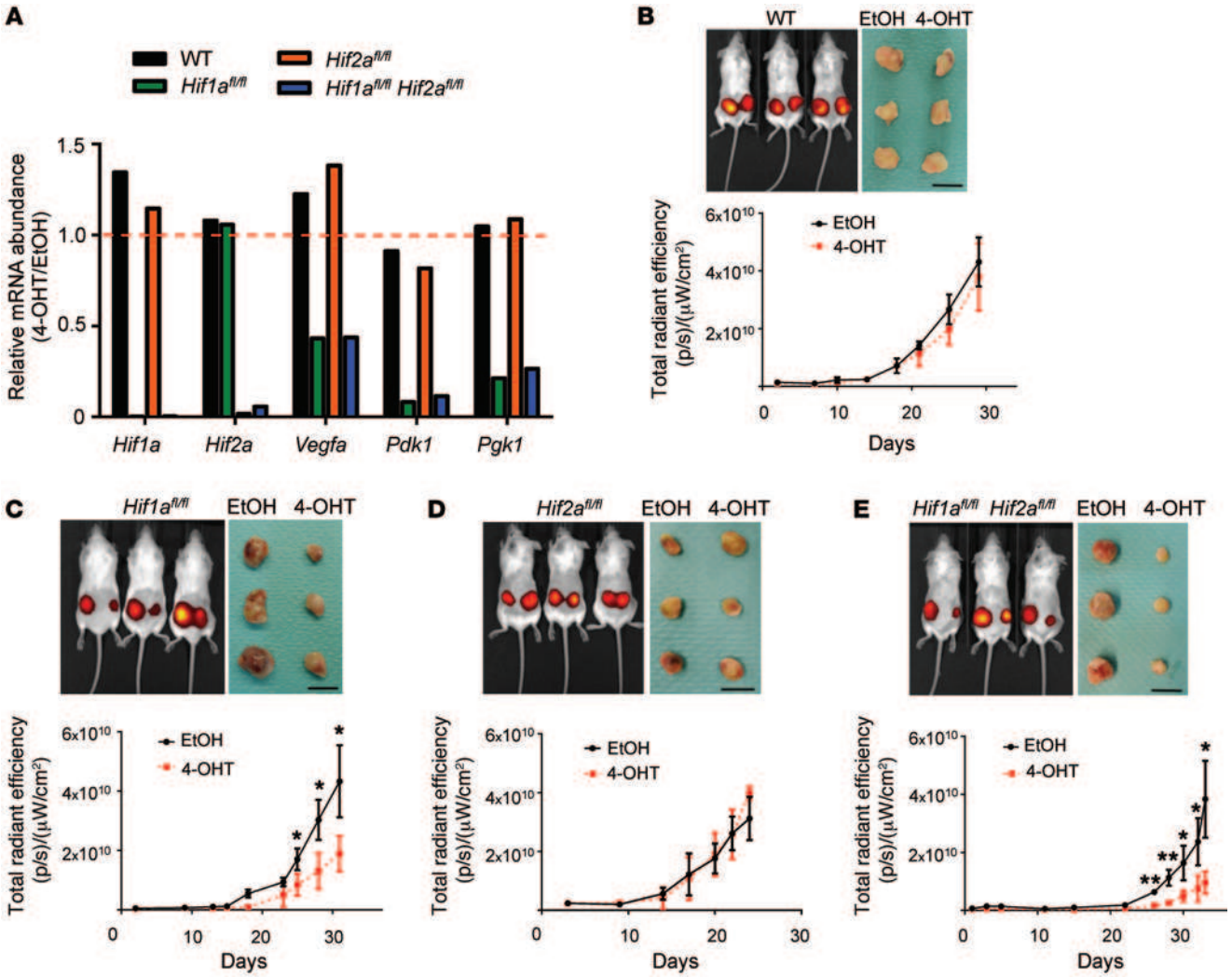

Figure 7. *Hif1a* but not *Hif2a* is necessary for efficient growth of *Pten*/*Rb1*-deficient, *H-Ras*^{G12V}–expressing tumors. (**A**) mRNA expression analysis of the indicated genes in WT, *Hif1a*$^{fl/fl}$, *Hif2a*$^{fl/fl}$, and *Hif1a*$^{fl/fl}$ *Hif2a*$^{fl/fl}$ MEFs that were transduced with lentivirus generated from the vector shown in Figure 6A 96 hours after induction of CreER^{T2} with 300 nm 4-OHT. Shown are ratios of 4-OHT treated to EtOH treated. (**B**–**E**) In vivo fluorescence imaging at the day of euthanasia (top left panels), excised tumors (top right panels), and longitudinal tumor growth (bottom panels) of mice injected with cells described in **A** that had been treated with EtOH (left flank) or 4-OHT (right flank) prior to subcutaneous injection. Color intensity in **B**–**E** is the same as in Figure 6C. Scale bars: 1 cm. All graphs depict mean ± SD. Student's *t* test, $n = 3–6$. $^*P < 0.05$; $^{**}P < 0.01$.

ing that combinatorial genetic manipulations via lentiviral injection can generate brain tumors (25), we tested whether autochthonous tumors could also be induced in mice via direct transduction of cells with MuLE viruses in vivo. Using R26-lox-STOP-lox-td-Tomato mice (26) as a reporter system to monitor cellular infection, we found that injection of ecotropic viruses expressing Cre into the gastrocnemius muscle of mice induced tdTomato fluorescence in muscle fibers and small cells adjacent to muscle fibers (Figure 10A). Mouse models have demonstrated that oncogenic *K-Ras* expression combined with loss of *Trp53* or *Cdkn2a* function in skeletal muscle cells of different stages of differentiation causes several types of soft tissue sarcomas, including embryonal and pleomorphic rhabdomyosarcomas (RMS) as well as undifferentiated pleomorphic sarcomas (UPS) with or without myogenic differentiation (27–30). The RAS-signaling pathway is frequently activated in childhood RMS tumors due to oncogenic mutations in the *HRAS*, *KRAS*, or *NRAS* genes or homozygous deletions of *NF1* (31–35). Some RMS tumors also harbor loss-of-function mutations or gene deletions in the *CDKN2A*, *TP53*, and *PTEN* genes (32–34, 36, 37), and systematic analysis of the status of the *TP53* and *CDKN2A* loci, as well as of their respective proteins, revealed that UPS tumors almost universally display loss of 1 or more components of the p53 pathway (38). To determine whether MuLE viruses could be utilized to model human sarcomas, we generated a series of MuLE vectors designed to systematically investigate the single and combinatorial effects of gain of *H-Ras* function and loss of *Cdkn2a*, *Trp53*, and *Pten* functions. All MuLE vectors expressed luciferase to mark infected cells, allowing quantitative monitoring of tumor development. Concentrated ecotropic lentiviruses (10^7 CFU/ml) were injected once into each gastrocnemius muscle of 18-day-old SCID/beige immunocompromised mice. Injection of empty control virus, viruses expressing only

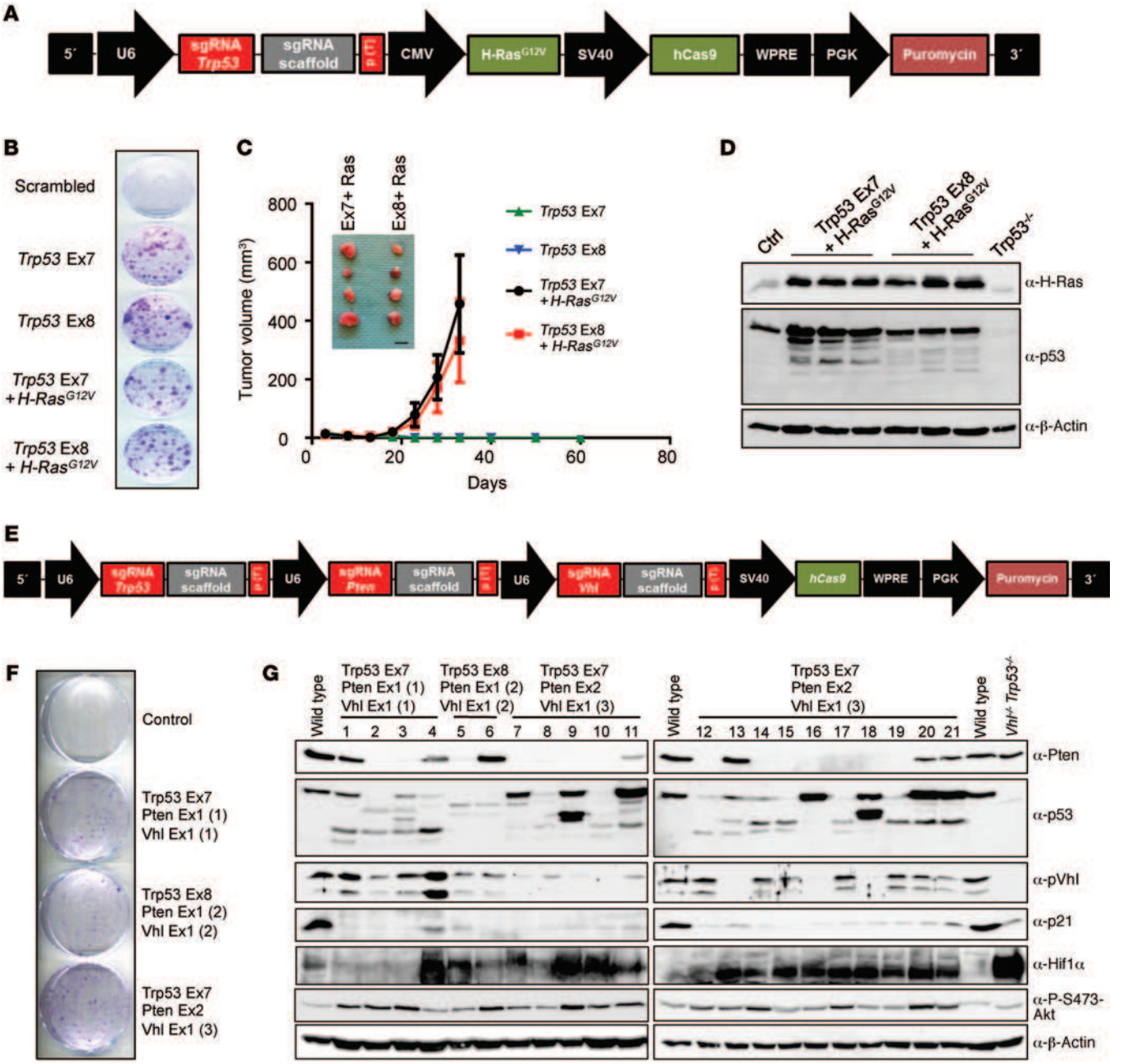

Figure 8. Combinatorial genetics using the CRISPR/Cas9 system in MuLE vectors. (**A**) Schematic of MuLE vector expressing sgRNA against *Trp53* and expressing *H-Ras^{G12V}*, *hCas9*, and puromycin resistance. (**B**) MEFs were infected with the indicated viruses expressing sgRNAs targeting *Trp53* exon 7 (Ex7) or exon 8 with or without *H-Ras^{G12V}* expression, plated at low density 6 days after transduction, and stained with crystal violet 14 days after plating. (**C**) Growth of cells as tumor xenografts and images of tumors derived from the combination of *Trp53* exon 7 or exon 8 sgRNAs with *H-Ras^{G12V}* overexpression. (**D**) Western blot analysis of tumor cells that were isolated from 3 separate tumors of each genotype 5 weeks after cell injection. (**E**) Schematic of MuLE vector simultaneously expressing sgRNAs against *Trp53*, *Pten*, and *Vhl* and expressing *hCas9* and puromycin resistance. (**F**) MEFs infected with 3 independent combinations of different sgRNAs formed colonies when plated at low density 10 days after viral transduction. (**G**) Western blotting of cell lines (lanes 1–21) derived from colonies that formed after infection with viruses expressing the indicated combinations of sgRNAs.

H-Ras^{G12V}, only shRNA-*Cdkn2a*, shRNA-*Trp53*, or shRNA-*Pten*, or viruses expressing shRNA-*Trp53* plus shRNA-*Pten* or shRNA-*Pten* plus *H-Ras^{G12V}* did not cause any large increases in luciferase signal over time (Figure 10, B and C), and no tumors developed within 4 months of injection. However, large increases in luciferase signal were evident in all muscles that were injected with shRNA-*Cdkn2a* plus *H-Ras^{G12V}* (n = 16), shRNA-*Trp53* plus *H-Ras^{G12V}* (n = 8), and shRNA-*Trp53* plus shRNA-*Pten* plus *H-Ras^{G12V}* (n = 6) combinatorial viruses as early as 10 days after injection (Figure 10, B and C). These signals increased over time, and all mice developed large tumors at the site of injection (Figure 10, D and E), requiring euthanasia of the animals 4 to 8 weeks after injec-

Table 1. Genotyping sequencing analysis of mutations at the *Pten*, *Trp53*, and *Vhl* loci in the indicated cell clones

Clone	*Pten* exon 2	*Trp53* exon 7	*Vhl* exon 1
WT	CTTGAAGGTGTATACAGGAACAATATT	AGCTCCTGCATGGGGGGCATGAACCGC	GGGCGGCCGCGGCCGGTGCTGCGCTCG
7	CTTGAAGGTGTAATACAGGAACAATATT	....27bp del.....CATGAACCGC	GGGCGGCC......GGTGCTGCGCTCG
	CTTGAAGGTG.TACAGGAACAATATT	AGCTCCTGCATTGGGGGGCATGAACCGC	GGGCGGCCGCCGGCCGGTGCTGCGCTCG
8	CTTGAAGGT....ACAGGAACAATATT	.........57bp del..........	GGGCGGCCGCGGC.GGTGCTGCGCTCG
	CTTGAAGGTGT.ACAGGAACAATATT	AGCTCC....TGGGGGGCATGAACCGC	GGGCGGCCGCGGCCGGTGCTGCGCTCG
9	CTTGAAGGTG....24 bp del.....	AGCTCCTGCAATGGGGGGCATGAACCGC	GGGCGGCCGCGGC......TGCGCTCG
	CTTGAAGGTGTAAATACAGGAACAATATT	AGCTCCTGC.TGGGGGGCATGAACCGC	GGGCGGCCG......GTGCTGCGCTCG
10	CTTGA..........AGGAACAATATT	A..............GCATGAACCGC	GGGCGGCCGC...CGGTGCTGCGCTCG
	CTTGAAGGTGT.ACAGGAACAATATT	AGCTCCTGCAATGGGGGGCATGAACCGC	GGGCGGCCGCGG.CGGTGCTGCGCTCG
14	CTTGAAGGTGTAATACAGGAACAATATT	AGCTCCTGCAATGGGGGGCATGAACCGC	GGGCGGCCGCG......GCTGCGCTCG
	CTTGAAGGTGTATTACAGGAACAATATT	AGCTCCTGCAATTTCC 136 bp ins	GGGCGGCCGCGGCCGGTGCTGCGCTCG
15	CTTGA..........AGGAACAATATT	AGCTCCTGCAT.GGGGGCATGAACCGC	GGGCGGCCGCG......GCTGCGCTCG
	CTTGAAGGTGTATTTACAGGAACAATATT	AGCTCCTGCAATGGGGGGCATGAACCGC	GGGCGGCCGCGGC.GGTGCTGCGCTCG
17	CTTGAAGGTGTATTACAGGAACAATATT	AGCTCCTGCAATGGGGGGCATGAACCGC	GGGCGGCCGCG......GCTGCGCTCG
	CTTGAAGGTGTATACAGGAACAATATT	AGCTCCTGCAATGGGGGGCATGAACCGC	GGGCGGCCGCGGC.GGTGCTGCGCTCG
18	.........32bp del..........	AGCTC...CATGGGGGGCATGAACCGC	GGGCGGCCGCGGC.GGTGCTGCGCTCG
	CTTGAAGGTGTAATACAGGAACAATATT	AGCTCCTGC.TGGGGGGCATGAACCGC	GGGCGGCCGCG......GCTGCGCTCG
19	C..............AGGAACAATATT	AGCTCCTGCAATGGGGGGCATGAACCGC	GG.....GCTCG
	CTTGAAGGTG.....ATATT	AGCTCCTGCAATGGGGGGCATGAACCGC	GGGCGGCCGCGGCCGGTGCTGCGCTCG
20	CTTGAAGGTG.....ATATT	12bp del.ATGGGGGGCATGAACCGC	GGGCGGCC...GCCGGTGCTGCGCTCG
	CTTGAAGGTGTAAATACAGGAACAATATT	AGCTCCTGCAATGGGGGGCATGAACCGC	GGGCGGCCGCGGCCGGTGCTGCGCTCG

The sequences of the 2 alleles of each locus are listed; underlined dots represent a base deletion and underlined text a base insertion compared with the WT sequence.

tion. Histological analysis of the tumors revealed that they were undifferentiated sarcomas with pleomorphic and rhabdoid features. Tumors contained undifferentiated round to spindle cells and an admixture of polygonal cells with densely eosinophilic cytoplasm in spindle, tadpole, and racquet-like contours (Figure 10, F–K). The presence of pleomorphic polygonal rhabdoid cells (Figure 10, G, I, and K) and the demonstration by electron microscopy of rudimentary sarcomere formation in the malignant cells (Figure 10, L and M) demonstrated myogenic differentiation in some cells. Injections of shRNA-*Cdkn2a* plus *H-Ras*^{G12V} MuLE viruses in C57BL/6 mice and Balb/c mice caused the development of sarcomas with kinetics and histology similar to those arising in SCID/beige mice (Supplemental Figure 8, A–C), demonstrating that MuLE viruses can also be employed to generate autochthonous tumors in immunocompetent mice. Independent cell lines were generated from multiple shRNA-*Cdkn2a* plus *H-Ras*^{G12V}, shRNA-*Trp53* plus *H-Ras*^{G12V}, and shRNA-*Trp53* plus shRNA-*Pten* plus *H-Ras*^{G12V} tumors. Western blotting confirmed H-Ras^{G12V} overexpression and reduction in protein abundance of p16, p19, p53, and PTEN in the respective genotypes (Figure 10O). While *Pten* knockdown led to clear induction of Akt phosphorylation at S473, no biological differences could be observed between tumors or cell lines with or without *Pten* knockdown. Tumor xenografts of these cell lines grew at similar rates (Supplemental Figure 8, D and E) and exhibited histologies indistinguishable from the original tumors (Supplemental Figure 8, F–H). These findings demonstrate that the MuLE system represents a powerful tool allowing the rapid and systematic generation of genetically complex, quantitatively monitorable autochthonous tumors and tumor-derived cancer cell lines in mice.

Discussion

We show proof-of-principle examples that illustrate the user friendliness, speed, versatility, and genetic power of the MuLE system in primary mammalian cells. Complex genetic modulations involving combinatorial gene overexpression, knockdown, and knockout can be achieved using single viral infections. The simultaneous marking of infected cells with a variety of reporter cassettes facilitates cellular studies and in vivo imaging studies. By expressing multiple sgRNAs together with hCas9, single MuLE vectors are able to simultaneously target genetic mutations to multiple loci, providing a platform that harnesses the genetic power of the CRISPR/Cas9 system for performing combinatorial genetic manipulations. Combinatorial genetic screening experiments are also possible by combining libraries of Entry vectors with Entry vectors that encode defined genetic alterations. The ease of combining different genetic elements using this system represents a tool that will greatly facilitate systematic combinatorial genetic studies in mammalian cells. Although this study focuses on tumor biology, the MuLE system will be widely applicable to numerous areas of biological investigation. It is hoped that other investigators will utilize the building-block nature of the system to generate new Entry vectors that will expand the range of possible genetic manipulations.

While there are several theoretical concerns that could potentially be envisaged as limiting the utility of complex MuLE lentiviruses, our data indicate that these do not represent significant problems. While some lentiviral vector plasmids are unstable in bacteria, MuLE vector plasmids are not prone to unwanted recombination during bacterial propagation. Another potential source of recombination in lentiviral vectors is at the level of

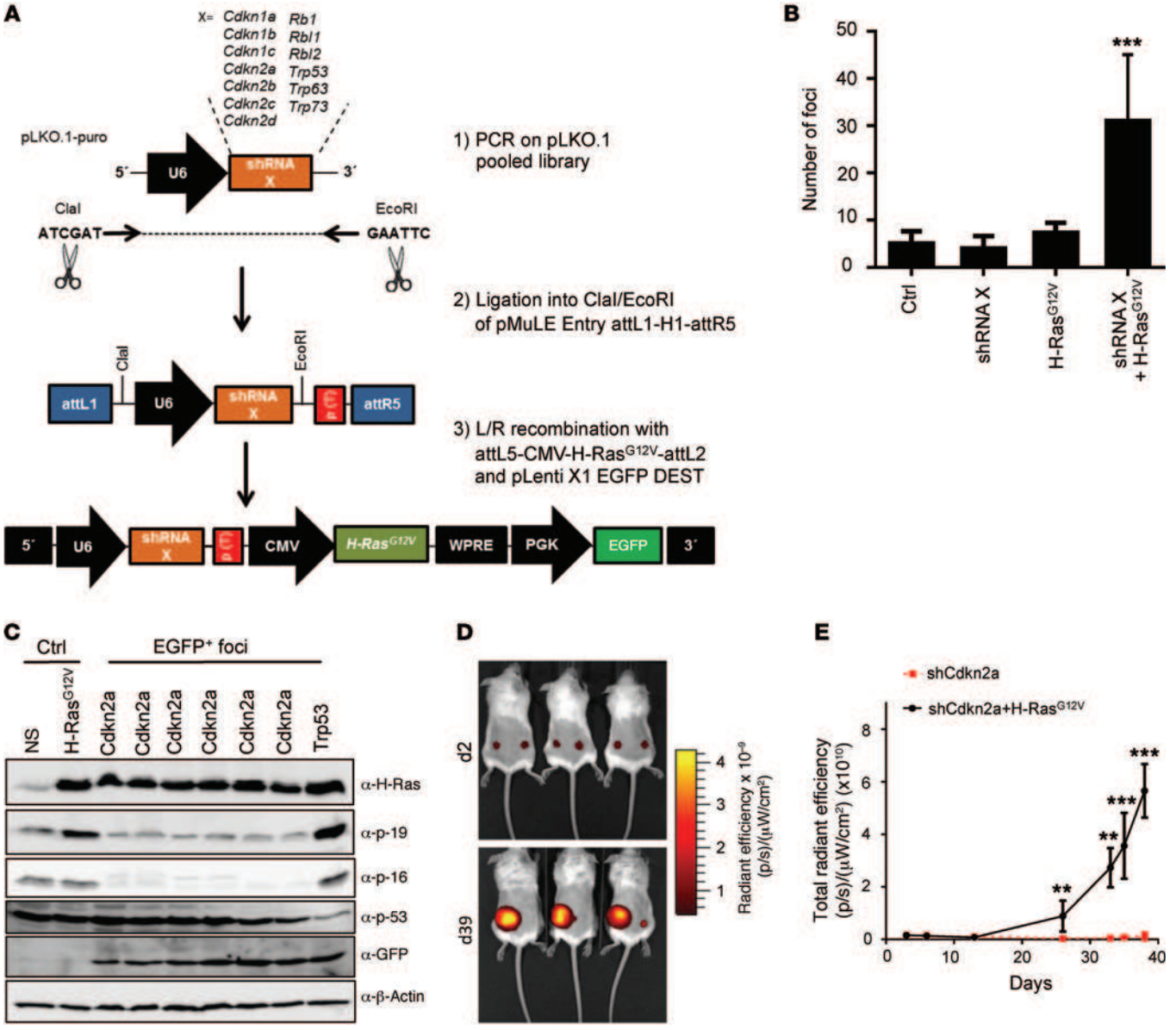

Figure 9. Combinatorial genetic screening using MuLE vectors. (**A**) Schematic representation of the workflow to generate a MuLE Entry vector shRNA library targeting the listed genes (shRNA X) and the final tricistronic lentiviral expression vector library that was used to screen for shRNAs that cause cell transformation in cooperation with oncogenic H-Ras^{G12V} overexpression. (**B**) Quantification of foci that were formed when WT MEFs were transduced with the indicted lentiviruses (MOI = 0.1). (**C**) Western blot analysis of EGFP-expressing cell clones derived from foci harboring shRNA against the indicated gene. (**D**) In vivo fluorescence images of mice that were subcutaneously injected with WT MEFs that had been infected with a MuLE virus expressing the identified shRNA against *Cdkn2a* alone plus iRFP or in combination with *H-Ras^{G12V}* and iRFP. (**E**) Tumor growth in the same mice monitored by longitudinal in vivo fluorescence imaging. All graphs depict mean ± SD. Student's *t* test, $n = 3$. $^{**}P < 0.01$; $^{***}P < 0.001$.

reverse transcription of the viral genome. Some studies have described that repeated genetic elements can undergo recombination-mediated deletion at low frequency in viral infections (39, 40), while other studies show that recombination of repeated elements was not detectable (41, 42). For this reason, we sought to provide options that would allow users to avoid the use of repeated elements in MuLE vectors in the unlikely event that unwanted recombination would prove to be an experimental problem. We generated Entry vectors with multiple different pol II and pol III promoters to allow gene and shRNA expression without incorporating repeated elements into final MuLE expression vectors. Our own experiments using repeated U6 promoter elements showed efficient knockdown or CRISPR/Cas9-mediated knockout of all genes that were targeted by the shRNAs or sgRNAs, suggesting that high levels of recombined viruses are not being produced in a manner that negatively affects achieving the desired genetic modulations. Another theoretical drawback of lentiviral vectors is the potential for insertional mutagenesis, although new generation HIV-based self-inactivating (SIN) lentiviral vectors (such as the vector that the MuLE system is based on) appear to not suffer from the problems of deleterious insertional mutagenesis that were observed with initial γ-retroviral gene-delivery vectors.

Lentiviral vectors have been shown to be safe in recent gene therapy trials (43, 44). Several lines of evidence demonstrate that random insertional mutagenesis of MuLE vectors does not contribute to the observed phenotypes in this study. Every experiment included all control vectors, including vectors with empty inserts, or expressing only single or double combinations of genes to control for potential effects of insertional mutagenesis. For example, as shown in Figure 4, E and F, cellular transformation and anchorage-independent growth only occurred when *Trp53* was knocked down together with *H-Ras*^{G12V} overexpression. Cells that were infected with MuLE viruses expressing only shRNA-*Trp53* or only *H-Ras*^{G12V} represent genetically sensitized cells that could be envisaged as being prone to oncogenic transformation by insertional mutagenesis. However, transformed cells that could grow in soft agar were never observed in these infections. Similarly, in all of the sarcoma tumor–modeling experiments, none of the relevant empty, single, and double control vectors induced tumors. Tumors arose rapidly in 100% of mice after injection of the shRNA-*Cdkn2a* plus *H-Ras*^{G12V}, shRNA-*Trp53* plus *H-Ras*^{G12V}, and shRNA-*Trp53* plus shRNA-*Pten* plus *H-Ras*^{G12V} combinatorial MuLE viruses with almost uniform kinetics, indicating that the tumors are driven by the genetic alterations introduced by the MuLE viruses and not as a result of rare random cooperating mutagenic events. One real practical limitation to the complexity of cloned MuLE vectors is that, as with all lentiviruses, viral titer decreases proportionally to the size of the provirus (Supplemental Figure 2 and ref. 45). In our hands, proviruses up to approximately 12 kb were able to generate experimentally usable viral titers; however, users are advised to generate the smallest possible proviruses if achieving a very high viral titer is experimentally important. The MuLE Entry vector toolbox is theoretically also compatible with other Gateway cloning–based plasmid and viral delivery systems, potentially allowing for larger and more complicated vectors and providing additional opportunities for targeting different cell types.

A great promise of the MuLE system is the potential to allow genetic manipulation of somatic cells directly in mice and potentially in other mammals. Bypassing extensive germline transgenic approaches has major benefits in terms of time and cost, and the lentiviral-mediated somatic genetics approach also mimics the fact that many cancer-associated genetic alterations are acquired in somatic cells. In this context, by engineering 3 new autochthonous mouse models of sarcoma, we show that MuLE viruses can be used to systematically assess the contribution of tumor suppressors and oncogenes to tumor formation in vivo. We show that the combinations of oncogenic *H-Ras*^{G12V} expression plus knockdown of *Cdkn2a*, *Trp53*, or both *Trp53* and *Pten* cause the formation of undifferentiated sarcomas with pleomorphic and rhabdoid features from skeletal muscles in mice. The histological similarity of these tumor models to existing transgenic mouse muscle–derived sarcoma models that are driven by oncogenic *K-Ras*^{G12V} in *Trp53* null, *Trp53* point mutant, or *Cdkn2a* null genetic backgrounds (27–30) demonstrates that MuLE viruses can be employed to recapitulate transgenic tumor models. Interestingly, additional *Pten* knockdown in shRNA-Trp53 plus *H-Ras*^{G12V} tumors caused phosphorylation of AKT, demonstrating hyperactivation of the PI3K pathway, but did not lead to any obvious differences in the phenotype of these tumors. It is noteworthy that *Trp53/Pten* double-knockdown or *Pten* knockdown plus *H-Ras*^{G12V} expression did not lead to tumor formation. These observations are potentially consistent with a recent report that activating *PIK3CA* and inactivating *PTEN* mutations in embryonal RMS mostly occur concurrently with mutations in *MYOD1* that functionally block myogenic differentiation (46). Thus, in muscle-derived sarcomas, the RAS and PI3K pathways appear to cooperate with different sets of genes to cause tumor formation.

The fact that MuLE-derived tumors are marked with luciferase and arise within weeks with uniform kinetics in every mouse will be advantageous for preclinical therapeutic studies, as tumor burden is quantitatively monitorable using a simple live-animal-imaging approach. In comparison, the generation of similar models using conventional genetic approaches would require the interbreeding of at least 4 to 5 different germline-modified transgenic mice (for example, tissue-specific Cre expression; homozygous floxed *Cdkn2a*, *Trp53*, and/or *Pten* alleles; Cre-inducible alleles of oncogenic *H-Ras*^{G12V}; and luciferase). The flexibility and speed of cloning that the MuLE system allows also paves the way for a systematic approach to model sarcomas by introducing other combinations of genetic alterations that occur in these tumor types, without the need for extensive crossing of germline-modified mice. By generating autochthonous tumors via direct injection of MuLE viruses into existing genetically modified mouse strains, it should also be possible to rapidly test, for example, the role of potential genetic modifiers or the immune system in tumor progression.

Lentiviral vectors allow gene transfer into dividing and nondividing cells and are increasingly being used for somatic cell transgenesis, including oncogene delivery (25, 47–49). The most common envelope protein used for pseudotyping lentiviral vectors is from vesicular stomatitis virus (VSV-G) and allows the infection of human cells (50, 51). Here, we have presented numerous examples of tumor engineering using the MuLE system, employing an ecotropic envelope protein from the Moloney murine leukemia virus (7, 52), which offers significant biosafety advantages (8). To the best of our knowledge, this envelope protein has not been previously employed for lentiviral delivery in vivo. In the context of tumor modeling in mice using lentiviral vectors that are potentially oncogenic in humans, the use of an ecotropic envelope prevents possible infection of researchers and also allows the use of conventional biosafety level 1 cell-culture and animal housing facilities, making this system available to almost all research groups. Our preliminary ex vivo and in vivo studies indicate that ecotropic MuLE viruses are able to transduce a wide variety of cell types, suggesting wide applicability of this system. Given the broad tropism of ecotropic MuLE viruses, achieving restricted infection of a particular cell type in vivo via a simple injection may not be possible in some settings. Our proof-of-principle demonstration that cell-type–specific expression can be achieved using a kidney-specific promoter element in the MuLE system may provide a solution to this issue. We also envisage that existing tissue-specific and/or inducible Cre, rtTA, and tTA mouse lines could provide the opportunity to spatially and temporally restrict gene expression from MuLE vectors containing *lox*P sites or tetracycline-responsive elements.

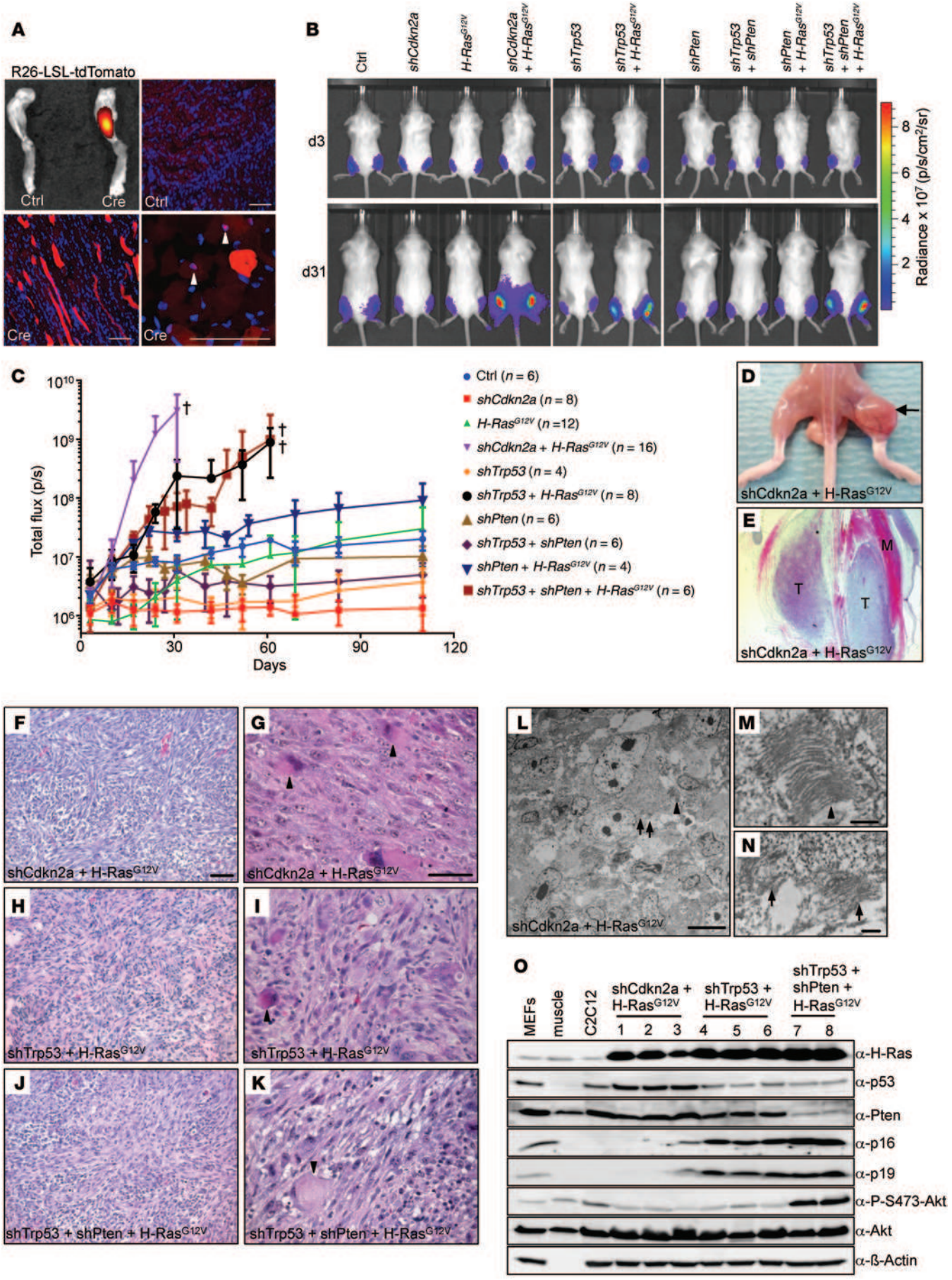
A
R26-LSL-tdTomato
Ctrl
Cre
Ctrl
Cre
Cre
B
Ctrl
shCdkn2a
H-Ras^{G12V}
shCdkn2a + H-Ras^{G12V}
shTrp53
shTrp53 + H-Ras^{G12V}
shPten
shTrp53 + shPten
shPten + H-Ras^{G12V}
shTrp53 + shPten + H-Ras^{G12V}
d3
d31
Radiance x 10^7 (p/s/cm^2/sr)
C
Total flux (p/s)
Days
Ctrl (n = 6)
shCdkn2a (n = 8)
H-Ras^{G12V} (n =12)
shCdkn2a + H-Ras^{G12V} (n = 16)
shTrp53 (n = 4)
shTrp53 + H-Ras^{G12V} (n = 8)
shPten (n = 6)
shTrp53 + shPten (n = 6)
shPten + H-Ras^{G12V} (n = 4)
shTrp53 + shPten + H-Ras^{G12V} (n = 6)
D
shCdkn2a + H-Ras^{G12V}
E
M
T
T
shCdkn2a + H-Ras^{G12V}
F
shCdkn2a + H-Ras^{G12V}
G
shCdkn2a + H-Ras^{G12V}
H
shTrp53 + H-Ras^{G12V}
I
shTrp53 + H-Ras^{G12V}
J
shTrp53 + shPten + H-Ras^{G12V}
K
shTrp53 + shPten + H-Ras^{G12V}
L
shCdkn2a + H-Ras^{G12V}
M
N
O
MEFs
muscle
C2C12
shCdkn2a + H-Ras^{G12V}
shTrp53 + H-Ras^{G12V}
shTrp53 + shPten + H-Ras^{G12V}
1 2 3 4 5 6 7 8
α-H-Ras
α-p53
α-Pten
α-p16
α-p19
α-P-S473-Akt
α-Akt
α-ß-Actin

Figure 10. Generation of 3 autochthonous mouse models of undifferentiated sarcoma using MuLE vectors. (**A**) Intramuscular injection of ROSA26-lox-STOP-lox-tdTomato mice with control or Cre-expressing virus. Bottom left panel shows infected myofibers, and small cells adjacent to myofibers are seen at higher magnification (arrowheads, bottom right panel). (**B**) Bioluminescence imaging 3 and 31 days after injection of 3×10^5 functional viral particles into each gastrocnemius muscle of 18-day-old SCID/beige mice with MuLE-luciferase viruses expressing combinations of shRNA against *Cdkn2a*, *Trp53*, and *Pten* with or without expression of *H-Ras*^{G12V}. (**C**) Quantification (mean ± SD) of luminescent signal intensities over time after injection. †Sacrifice of all mice in these cohorts by this time point. (**D**) A tumor (arrow) in a mouse injected with the sh*Cdkn2a* plus H-Ras^{G12V} MuLE virus only in the right gastrocnemius muscle. (**E**) Histological image of the tumor (T) from **D** surrounded by muscle tissue (M). (**F**–**K**) Representative histology of tumors derived from injection of shCdkn2a plus H-Ras^{G12V} (**F** and **G**), shTrp53 plus H-Ras^{G12V} (**H** and **I**), and shTrp53 plus shPTEN plus H-Ras^{G12V} (**J** and **K**) viruses. Arrowheads in **G**, **I**, and **K** highlight pleomorphic rhabdoid cells. (**L**) EM showing an example of a tumor cell with sarcomere formation; **M** and **N** show higher magnification of the regions in **L** marked with an arrowhead and arrows, respectively, showing Z-bands or irregular masses of Z-band material with converging filaments. (**O**) Western blot analysis of independent cell lines (lanes 1–8) derived from independent tumors of the indicated genotypes. MEFs, muscle tissue, and C2C12 myoblast cells served as controls. Scale bars: 50 μm (**A** and **F**–**K**); 10 μm (**L**); 500 nm (**M** and **N**).

Methods

Cells. Primary MEFs were isolated from relevant WT or floxed strains and were frozen in aliquots at passage 2. MEFs were cultured in DMEM plus 10% FCS in cell-culture incubators supplemented with 5% CO_2 and maintained at 5% O_2. If not stated otherwise, cells were transduced at a MOI between 1 and 2. MEFs were incubated overnight in virus-containing medium in the presence of 4 μg/ml polybrene (Sigma-Aldrich, no. H9268). Drug selection was performed 48 hours after transduction using the following concentrations: 3 μg/ml puromycin, 10 μg/ml blasticidin, 500 μg/ml G418. Human melanoma A-375 cells (ATCC, no. CRL-1619) were cultured in DMEM plus 10% FCS. C2C12 cells were obtained from Sigma-Aldrich (no. 91031101) and cultured in DMEM plus 15% FCS. HEK293T (ATCC, no. CRL3216) and NIH3T3 cells (ATCC, no. CRL-1658) were cultured in DMEM plus 10% FCS. LLC-1, B16-F10, and MC-38 cell lines were a gift of Lubor Borsig (Institute of Physiology, University of Zurich) and cultured in DMEM plus 10% FCS. Mouse embryonic stem cells were a gift of Kurt Bürki (Institute of Physiology, University of Zurich) and cultured in N2B27+ 2i medium. Murine primary kidney epithelial cells were isolated and cultured as described before (53). Endometrial epithelial cells were isolated and cultured as described (54). Murine aortic endothelial cells and immortalized mouse hepatocytes were gifts of Rok Humar (Research Unit, Division of Internal Medicine, University Hospital of Zurich, Zurich, Switzerland) and Nora Rösch (Institute of Molecular Health Sciences, ETH Zurich, Zurich, Switzerland), respectively, and were cultured in DMEM plus 10% FCS. Cells were isolated from dissected tumors by digestion for 1 hour at 37°C with 1 mg/ml collagenase type II (Gibco; Life Technologies), washed twice with PBS, and cultured in DMEM plus 10% FCS. All cells were kept in cell-culture incubators supplemented with 5% CO_2 and maintained at 20% O_2.

Cloning of MuLE vectors. Details of the cloning of all parental MuLE Entry and Destination vectors, the experimental Entry vectors, and experimental MuLE expression vectors that were used in this study are provided in Supplemental Methods.

Cloning of sgRNAs, surveyor assays, and next generation sequencing. Design and cloning of sgRNAs used in this study are described in Supplemental Methods. For Surveyor assays, 350- to 450-bp fragments surrounding the sgRNA target site were amplified using proof-reading PCR (Expand High Fidelity, Roche). Primers and PCR conditions are described in Supplemental Methods. For mixed cell populations, heteroduplexes were formed by reannealing the PCR product alone by heating to 95°C followed by gradual cooling. Heteroduplexes were digested with Surveyor nuclease (7 μl heteroduplex, 1 μl Surveyor Enhancer S, 1 μl Surveyor Nuclease S, 1 μl 0.15 M $MgCl_2$) for 60 minutes at 42°C and subjected to 10% polyacrylamide gel electrophoresis using 1× TBE as running buffer. For sequencing of the *Trp53*, *Vhl*, and *Pten* loci in cell clones, gene segments surrounding the sgRNA-binding site were amplified from genomic DNA using primers described in Supplemental Methods, followed by ligation to barcoded adaptors and pooled sequencing using Ion Torrent PGM. The full protocol is provided in Supplemental Methods. Sequencing data were deposited in the NCBI's BioProject database (ID 272478).

Lentivirus production and titration. Lentivirus was prepared using calcium phosphate-mediated transfection of subconfluent HEK293T cells cultured in DMEM plus 10% FCS. For a 10-cm dish, lentiviral vector (8 μg) was cotransfected with the lentiviral packaging vector psPAX2 (Addgene, no. 12260) and either the ecotropic envelope (pCMV-Eco, Cellbiolabs, no. RV-112) or the amphotropic envelope (pMD2.G, Addgene, no. 12259). Concentration of lentiviral particles for in vivo injection was done via centrifugation for 5 hours at 11,000 *g* over a layer of 20% sucrose (55). In cases in which the viral construct contained a drug-resistance gene, determination of functional viral titer was performed by drug-resistance colony assay with NIH3T3 cells as described (56). In cases in which fluorescent reporters expressed from the constructs, titers were determined using FACS as described (56). For determination of titers with luciferase as the only reporter, we generated an EGFP-luciferase–expressing lentiviral vector and used this to generate a reference curve, which allowed us to determine the titer of viruses by measuring luciferase activity in cells that had been transduced with different dilutions of the virus.

Antibodies, Western blotting, and immunohistochemistry. Western blotting and immunohistochemistry were conducted as described (57) using antibodies against the following epitopes: H-Ras (Santa Cruz Biotechnology Inc., no. sc-520), β-actin (Sigma-Aldrich, A2228), p16 (Santa Cruz Biotechnology Inc., no. sc-1207), p19 (Santa Cruz Biotechnology Inc., no. sc-32748), Myc (Sigma-Aldrich, no. M5546), VHL (Santa Cruz Biotechnology Inc., sc-5575), p53 (Novocastra, NCL-p53-CM5p), PTEN (Santa Cruz Biotechnology Inc., no. sc-7974), GFP (Life Technologies, no. G10362), Rb1 (Cell Signaling, no. 9313), HIF1α (Novus, no. NB100-479), p21 (F5) (no. sc-6246), phospho-Akt (Ser473) (193H12) (Cell Signaling, no. 4058), and Akt (pan) (C67E7) (Cell Signaling no. 4691). The full scans of all Western blots are available in the Supplemental Material.

Real-time PCR. Real-time PCR was performed as described (57) using the following primer pairs: *S12* (5′-GAAGCTGCCAAAGCCTTAGA-3′, 5′-AACTGCAACCAACCACCTTC-3′), *Hif1a* (5′-TGCTCATCAGTTGCCACTTC-3′, 5′-CCTCATGGTCACATGGATGA-3′), *Hif2a* (5′-GAGGAAGGAGAAATCCCGTGA-3′, 5′-CTGATGGCCAGGCGCATGATG-3′), *Vegfa* (5′-CTTGTTCAGAGCGGAGAAAGC-3′, 5′-ACATCTGCAAGTACGTTCATT-3′), *Pdk1* (5′-GGACTTCGGGTCAGTGAATGC-3′, 5′-TCCTGAGAAGATTGTCGGGGA-3′), and *Pgk1* (5′-TGCTGCTGAACTCAAATCTCTG-3′, 5′-CAGGCATTCTCGACTTCTGGG-3′).

In vivo imaging. Noninvasive in vivo multispectral fluorescence and bioluminescence imaging were performed using the IVIS Spectrum (PerkinElmer) with Living Image software (version 4.4). Mice were anesthetized using a vapor isoflurane inhalation narcosis system. For narcosis initiation, 3% isoflurane (Attane, MINRAD Inc.) in O_2 at a flow rate of 3 to 5 μl/min was given via an inhalation mask with the mouse placed on a warming plate. During imaging, the isoflurane levels were reduced to 1% to 2%. For fluorescence time-course measurements of tumor xenografts, mice were shaved and imaged at the indicated time points after cell injection. The filter channels used for calculation of tumor growth with iRFP were Ex.675/Em.725 and for mCherry Ex.570/Em.620. All measurements were performed in epifluorescence mode if not otherwise stated. For the quantification of the total radiant efficiency, a region of interest was drawn around the tumor and total radiant efficiency was measured. For bioluminescence imaging, mice were injected subcutaneously with 150 mg/kg D-luciferin (Caliper, no. 122796) and imaged when peak signal intensities were reached, usually 13 to 17 minutes after injection.

Mice. SCID/beige mutant mice (*C.B-17/CrHsd-Prkdc^{scid}Lyst^{bg-J}*) and C57BL/6 and BALB/c mice were obtained from Harlan Laboratories and housed under standard conditions. *Vhl$^{fl/fl}$ Trp53$^{fl/fl}$*, *Pten$^{fl/fl}$*, *Hif1a$^{fl/fl}$*, and *Hif2a$^{fl/fl}$* mice have been previously described (53, 58–60). B6.Cg-*Gt(ROSA)26Sor$^{tm14(CAG-tdTomato)Hze}$*/J mice were obtained from Jackson Laboratory (stock no. 007914). For xenograft experiments, mice were anesthetized and injected subcutaneously with 5×10^6 cells suspended in 50% Matrigel (BD, no. 354230). In parallel to in vivo imaging studies, tumor size was measured using a caliper. For intramuscular injections of lentiviruses, 18- to 20-day-old juvenile mice were anesthetized and injected with concentrated ecotropic lentivirus into the gastrocnemius muscle.

Statistics. Statistical significance was determined by 2-tailed Student's *t* test, with a *P* value of less than 0.05 considered to be statistically significant.

Study approval. All mouse experiments were approved by the Veterinary Office of the Canton of Zurich under the licences 06/2013, 45/2010 and 137/2013.

Acknowledgments

We thank Lukas Sommer and Gaetana Restivo for helpful discussions regarding xenograft experiments. I.J. Frew is supported by grants from the Swiss National Science Foundation (Förderungsprofessur) and a European Research Council starting grant (260316). J. Albers received support from the European Community's Seventh Framework Programme under grant agreement no. 246539.

Address correspondence to: Ian Frew, Institute of Physiology, University of Zurich, Winterthurerstrasse 190, CH-8057 Zurich, Switzerland. Phone: 41.44.635.5004; E-mail: ian.frew@access.uzh.ch.

1. Ciriello G, Miller ML, Aksoy BA, Senbabaoglu Y, Schultz N, Sander C. Emerging landscape of oncogenic signatures across human cancers. *Nat Genet*. 2013;45(10):1127–1133.
2. Lawrence MS, et al. Discovery and saturation analysis of cancer genes across 21 tumour types. *Nature*. 2014;505(7484):495–501.
3. Dow LE, Lowe SW. Life in the fast lane: mammalian disease models in the genomics era. *Cell*. 2012;148(6):1099–1109.
4. Katzen F. Gateway recombinational cloning: a biological operating system. *Expert Opin Drug Discov*. 2007;2(4):571–589.
5. Paddison PJ, et al. Cloning of short hairpin RNAs for gene knockdown in mammalian cells. *Nat Methods*. 2004;1(2):163–167.
6. Campeau E, et al. A versatile viral system for expression and depletion of proteins in mammalian cells. *PLoS One*. 2009;4(8):e6529.
7. Tsai SQ, et al. Dimeric CRISPR RNA-guided FokI nucleases for highly specific genome editing. *Nat Biotechnol*. 2014;32(6):569–576.
8. Schambach A, et al. Lentiviral vectors pseudotyped with murine ecotropic envelope: increased biosafety and convenience in preclinical research. *Exp Hematol*. 2006;34(5):588–592.
9. Boiko AD, Porteous S, Razorenova OV, Krivokrysenko VI, Williams BR, Gudkov AV. A systematic search for downstream mediators of tumor suppressor function of p53 reveals a major role of BTG2 in suppression of Ras-induced transformation. *Genes Dev*. 2006;20(2):236–252.
10. Brosh R, Rotter V. When mutants gain new powers: news from the mutant p53 field. *Nat Rev Cancer*. 2009;9(10):701–713.
11. Prendergast GC. Mechanisms of apoptosis by c-Myc. *Oncogene*. 1999;18(19):2967–2987.
12. Filonov GS, Krumholz A, Xia J, Yao J, Wang LV, Verkhusha VV. Deep-tissue photoacoustic tomography of a genetically encoded near-infrared fluorescent probe. *Angew Chem Int Ed Engl*. 2012;51(6):1448–1451.
13. Filonov GS, Piatkevich KD, Ting L, Zhang J, Kim K, Verkhusha VV. Bright and stable near-infrared fluorescent protein for in vivo imaging. *Nat Biotechnol*. 2011;29(8):757–761.
14. Hock AK, Lee P, Maddocks OD, Mason SM, Blyth K, Vousden KH. iRFP is a sensitive marker for cell number and tumor growth in high-throughput systems. *Cell Cycle*. 2013;13(2):1–7.
15. Hsu PD, Lander ES, Zhang F. Development and applications of CRISPR-Cas9 for genome engineering. *Cell*. 2014;157(6):1262–1278.
16. Sander JD, Joung JK. CRISPR-Cas systems for editing, regulating and targeting genomes. *Nat Biotechnol*. 2014;32(4):347–355.
17. Sanchez-Rivera FJ, et al. Rapid modelling of cooperating genetic events in cancer through somatic genome editing. *Nature*. 2014;516(7531):428–431.
18. Xue W, et al. CRISPR-mediated direct mutation of cancer genes in the mouse liver. *Nature*. 2014;514(7522):380–384.
19. Maddalo D, et al. In vivo engineering of oncogenic chromosomal rearrangements with the CRISPR/Cas9 system. *Nature*. 2014;516(7531):423–427.
20. Platt RJ, et al. CRISPR-Cas9 knockin mice for genome editing and cancer modeling. *Cell*. 2014;159(2):440–455.
21. Malina A, et al. Repurposing CRISPR/Cas9 for in situ functional assays. *Genes Dev*. 2013;27(23):2602–2614.
22. Yang H, Wang H, Shivalila CS, Cheng AW, Shi L, Jaenisch R. One-step generation of mice carrying reporter and conditional alleles by CRISPR/Cas-mediated genome engineering. *Cell*. 2013;154(6):1370–1379.
23. Heckl D, et al. Generation of mouse models of myeloid malignancy with combinatorial genetic lesions using CRISPR-Cas9 genome editing. *Nat Biotechnol*. 2014;32(9):941–946.
24. Kuilman T, Michaloglou C, Mooi WJ, Peeper DS. The essence of senescence. *Genes Dev*. 2010;24(22):2463–2479.
25. Friedmann-Morvinski D, et al. Dedifferentiation of neurons and astrocytes by oncogenes can induce gliomas in mice. *Science*. 2012;338(6110):1080–1084.
26. Madisen L, et al. A robust and high-throughput Cre reporting and characterization system for the whole mouse brain. *Nat Neurosci*. 2010;13(1):133–140.
27. Tsumura H, Yoshida T, Saito H, Imanaka-Yoshida K, Suzuki N. Cooperation of oncogenic K-ras and p53 deficiency in pleomorphic rhabdomyosarcoma development in adult mice. *Oncogene*. 2006;25(59):7673–7679.
28. Rubin BP, et al. Evidence for an unanticipated relationship between undifferentiated pleomorphic sarcoma and embryonal rhabdomyosarcoma. *Cancer Cell*. 2011;19(2):177–191.
29. Hettmer S, et al. Sarcomas induced in discrete subsets of prospectively isolated skeletal muscle cells. *Proc Natl Acad Sci U S A*. 2011;108(50):20002–20007.
30. Blum JM, et al. Distinct and overlapping sarcoma subtypes initiated from muscle stem and progenitor cells. *Cell Rep*. 2013;5(4):933–940.
31. Chen X, et al. Targeting oxidative stress in embryonal rhabdomyosarcoma. *Cancer Cell*. 2013;24(6):710–724.
32. Martinelli S, et al. RAS signaling dysregulation in

human embryonal Rhabdomyosarcoma. *Genes Chromosomes Cancer*. 2009;48(11):975–982.
33. Paulson V, et al. High-resolution array CGH identifies common mechanisms that drive embryonal rhabdomyosarcoma pathogenesis. *Genes Chromosomes Cancer*. 2011;50(6):397–408.
34. Shern JF, et al. Comprehensive genomic analysis of rhabdomyosarcoma reveals a landscape of alterations affecting a common genetic axis in fusion-positive and fusion-negative tumors. *Cancer Discov*. 2014;4(2):216–231.
35. Shukla N, et al. Oncogene mutation profiling of pediatric solid tumors reveals significant subsets of embryonal rhabdomyosarcoma and neuroblastoma with mutated genes in growth signaling pathways. *Clin Cancer Res*. 2012;18(3):748–757.
36. Iolascon A, et al. Analysis of cyclin-dependent kinase inhibitor genes (CDKN2A, CDKN2B, and CDKN2C) in childhood rhabdomyosarcoma. *Genes Chromosomes Cancer*. 1996;15(4):217–222.
37. Kohashi K, et al. Alterations of RB1 gene in embryonal and alveolar rhabdomyosarcoma: special reference to utility of pRB immunoreactivity in differential diagnosis of rhabdomyosarcoma subtype. *J Cancer Res Clin Oncol*. 2008;134(10):1097–1103.
38. Perot G, et al. Constant p53 pathway inactivation in a large series of soft tissue sarcomas with complex genetics. *Am J Pathol*. 2010;177(4):2080–2090.
39. McIntyre GJ, et al. Cassette deletion in multiple shRNA lentiviral vectors for HIV-1 and its impact on treatment success. *Virol J*. 2009;6:184.
40. An W, Telesnitsky A. Frequency of direct repeat deletion in a human immunodeficiency virus type 1 vector during reverse transcription in human cells. *Virology*. 2001;286(2):475–482.
41. ter Brake O, Konstantinova P, Ceylan M, Berkhout B. Silencing of HIV-1 with RNA interference: a multiple shRNA approach. *Mol Ther*. 2006;14(6):883–892.
42. ter Brake O, t Hooft K, Liu YP, Centlivre M, von Eije KJ, Berkhout B. Lentiviral vector design for multiple shRNA expression and durable HIV-1 inhibition. *Mol Ther*. 2008;16(3):557–564.
43. Biffi A, et al. Lentiviral hematopoietic stem cell gene therapy benefits metachromatic leukodystrophy. *Science*. 2013;341(6148):1233158.
44. Aiuti A, et al. Lentiviral hematopoietic stem cell gene therapy in patients with Wiskott-Aldrich syndrome. *Science*. 2013;341(6148):1233151.
45. Kumar M, Keller B, Makalou N, Sutton RE. Systematic determination of the packaging limit of lentiviral vectors. *Hum Gene Ther*. 2001;12(15):1893–1905.
46. Kohsaka S, et al. A recurrent neomorphic mutation in MYOD1 defines a clinically aggressive subset of embryonal rhabdomyosarcoma associated with PI3K-AKT pathway mutations. *Nat Genet*. 2014;46(6):595–600.
47. Maeder ML, Linder SJ, Cascio VM, Fu Y, Ho QH, Joung JK. CRISPR RNA-guided activation of endogenous human genes. *Nat Methods*. 2013;10(10):977–979.
48. Siwko SK, et al. Lentivirus-mediated oncogene introduction into mammary cells in vivo induces tumors. *Neoplasia*. 2008;10(7):653–662.
49. Xia Y, et al. Reduced cell proliferation by IKK2 depletion in a mouse lung-cancer model. *Nat Cell Biol*. 2012;14(3):257–265.
50. Zufferey R, et al. Self-inactivating lentivirus vector for safe and efficient in vivo gene delivery. *J Virol*. 1998;72(12):9873–9880.
51. Dull T, et al. A third-generation lentivirus vector with a conditional packaging system. *J Virol*. 1998;72(11):8463–8471.
52. Hwang WY, et al. Efficient genome editing in zebrafish using a CRISPR-Cas system. *Nat Biotechnol*. 2013;31(3):227–229.
53. Albers J, et al. Combined mutation of Vhl and Trp53 causes renal cysts and tumours in mice. *EMBO Mol Med*. 2013;5(6):949–964.
54. Grant KS, Wira CR. Effect of mouse uterine stromal cells on epithelial cell transepithelial resistance (TER) and TNFα and TGFβ release in culture. *Biol Reprod*. 2003;69(3):1091–1098.
55. Romanowska M, Haritonova N, Foerster J. Optimized production and concentration of lentiviral vectors containing large inserts. *J Gene Med*. 2007;9(7):579–584.
56. Tonini T, Claudio PP, Giordano A, Romano G. Determination of functional viral titer by drug-resistance colony assay, expression of green fluorescent protein, and beta-galactoside staining. *Methods Mol Biol*. 2004;285:149–153.
57. Frew IJ, et al. pVHL and PTEN tumour suppressor proteins cooperatively suppress kidney cyst formation. *EMBO J*. 2008;27(12):1747–1757.
58. Groszer M, et al. Negative regulation of neural stem/progenitor cell proliferation by the Pten tumor suppressor gene in vivo. *Science*. 2001;294(5549):2186–2189.
59. Gruber M, Hu CJ, Johnson RS, Brown EJ, Keith B, Simon MC. Acute postnatal ablation of Hif-2alpha results in anemia. *Proc Natl Acad Sci U S A*. 2007;104(7):2301–2306.
60. Ryan HE, et al. Hypoxia-inducible factor-1alpha is a positive factor in solid tumor growth. *Cancer Res*. 2000;60(15):4010–4015.